Maintenance of spatial gene expression by Polycomb-mediated repression after formation of a vertebrate body plan

Authors: Julien Rougeot[1,2], Naomi D. Chrispijn[1], Marco Aben[1,2], Dei M. Elurbe[1,2], Karolina M. Andralojc[1], Patrick J. Murphy[3], Pascal W.T.C. Jansen[4], Michiel Vermeulen[4], Bradley R. Cairns[3], Leonie M. Kamminga[1,2,*]

Affiliations: [1]Radboud University, Faculty of Science, Department of Molecular Biology, Radboud Institute for Molecular Life Sciences, Nijmegen, the Netherlands [2]Radboud University Medical Center, Department of Molecular Biology, Nijmegen, the Netherlands [3]Howard Hughes Medical Institute, Department of Oncological Sciences and Huntsman Cancer Institute, University of Utah School of Medicine, Salt Lake City, UT 84112, USA [4] Radboud University, Department of Molecular Biology, Faculty of Science, Radboud Institute for Molecular Life Sciences, Oncode Institute, Nijmegen, The Netherlands. *Corresponding author.

Contact information:

Leonie Kamminga

Faculty of Science - Department of Molecular Biology

Geert Grooteplein 28

6525 GA Nijmegen

The Netherlands

Internal postal code 274

T +31 24 361 6850

l.kamminga@science.ru.nl

Abstract

Polycomb group proteins are transcriptional repressors that are important regulators of cell fate during embryonic development. Among them, Ezh2 is responsible for catalyzing the epigenetic repressive mark H3K27me3 and is essential for animal development. The ability of zebrafish embryos lacking both maternal and zygotic *ezh2* to form a normal body plan provides a unique model to comprehensively study Ezh2 function during early development in vertebrates. By using a multi-omics approach, we found that Ezh2 is required for the recruitment of H3K27me3 and Polycomb group protein Rnf2. However, in absence of Ezh2, only minor changes in global H3K4me3 levels and gene and protein expression occurred. These changes were mainly due to local deregulation of transcription factors outside their normal expression boundaries. Altogether, our results in zebrafish show that Polycomb-mediated gene repression is important only after the body plan is formed to maintain spatially restricted transcriptional profiles of Polycomb-targeted transcription factors.

Introduction

Development of multi-cellular organisms involves highly dynamic and controlled processes during which one single totipotent cell will multiply and differentiate into all the cells composing the adult individual. Specification of cell identity is controlled through the establishment of spatially and temporally restricted transcriptional profiles, which are subsequently maintained by epigenetic mechanisms(1). Epigenetic maintenance of gene expression can act through modifications of the chromatin, the complex of DNA wrapped around an octamer of histones H2A, H2B, H3, and H4 and its associated proteins and non-coding RNAs, creating an epigenetic landscape, often referred to as the epigenome(2). These modifications can be propagated from mother to daughter cells and thereby maintain gene expression profiles by controlling the accessibility of the DNA to the transcriptional machinery(3).

Important regulators of the epigenome during development are the Polycomb Group (PcG) proteins. First identified in *Drosophila melanogaster*, PcG proteins were found to maintain the pre-established pattern of *hox* gene expression(4). Subsequent studies showed that PcG proteins are important for proper patterning during early embryonic development, tissue-specific development, and maintenance of the balance between pluripotency and differentiation of stem cells in multiple species(5). Two main PcG complexes have been described(6). The Polycomb Repressive Complex 2 (PRC2) is composed of the core subunits EZH1/2 (Enhancer of Zeste Homologue 1/2), SUZ12 (Supressor of Zeste 12), and EED (Embryonic Ectoderm Development). EZH2 has a catalytically active SET domain that trimethylates lysine 27 of histone H3 (H3K27me3), an epigenetic mark associated with gene repression and found along gene coding sequences(7). The catalytic subunits of PRC2 are mutually exclusive and EZH1 is postulated to complement the function of EZH2 in non-proliferative adult organs(8, 9). H3K27me3 can be recognized by the Polycomb Repressive Complex 1 (PRC1). A diversity of PRC1 compositions has been described and canonical PRC1 is composed of the core subunits RING1/RNF2 (Ring Finger Protein 2 a/b), PCGF1-6 (Polycomb Group RING fingers 1-6), PHC

(Polyhomeotic), and CBX (Chromobox homolog)(10, 11). PRC1 catalyzes the ubiquitination of lysine 119 of histone H2A (H2AK1119ub) and strengthens gene repression. In contrast to this canonical view, recent studies implicate that PRC1 is also active in the absence of PRC2(12-14).

Trithorax Group (TrxG) proteins antagonize PcG protein function through the deposition of a trimethyl group on lysine 4 of histone H3 (H3K4me3) on promoters and enhancers from virtually all transcribed genes(15-17). Acetylation of H3K27 (H3K27ac) is a different epigenetic mark associated with promoters and active enhancers and constitutes a dynamic signature marking developmentally regulated genes(18).

In mice, loss of PRC2 genes *Ezh2*, *EED*, or *Suz12* or PRC1 gene *Rnf2* leads to post-implantation embryonic lethality during early gastrulation(19-22), making it difficult to study transcriptional regulation by PcG complexes during early development. Lately, the zebrafish embryo has emerged as a model of choice to study developmental epigenetics in vertebrates, although epigenomics studies on mutant lines are still rare(23-26). Others and we previously showed that *ezh2* is essential for zebrafish development(27-29). More particularly, zebrafish embryos mutant for both maternal and zygotic *ezh2*, referred as *MZezh2* mutant embryos, develop seemingly normal until 1 dpf, forming a proper body plan. These mutants ultimately die at 2 dpf, exhibiting a 100% penetrant pleiotropic phenotype associated with a loss of tissue maintenance(28). This makes zebrafish *MZezh2* mutant embryos a unique model to study the function of Ezh2 during early development, from fertilization to tissue specification, in the unique context of a vertebrate embryo in which trimethylation of H3K27 has never occurred, unlike cell culture, conditional, or zygotic mutant models.

We conducted a multi-omics approach in these *MZezh2* mutant embryos to study how PcG-mediated gene regulation controls axis formation and tissue specification. We focused our study on 24 hours post fertilization (hpf) embryos, when the first phenotypes become visible, and the anterior-posterior patterning of the embryos is properly established. Surprisingly, our data show

that, despite the complete absence of PcG associated epigenetic mark and proteins, the transcriptional and proteomic profile in *MZezh2* mutant embryos remains largely unchanged compared to wildtype embryos. The changes mainly affect transcription factors essential for developmental processes. Closer analysis of spatial expression of the genes deregulated in *MZezh2* mutants revealed that aberrant gene expression is primarily local. Our results show that zebrafish embryo development is initially independent of PcG repression until the stage of tissue maintenance, where PcG proteins maintain precise spatial repression of transcription factor expression.

Results

The repressive epigenetic mark H3K27me3 is absent in *MZezh2* embryos

To study the function of Ezh2 during development, we used the *ezh2* nonsense mutant allele *ezh2(hu5670)* containing a premature stop codon within the catalytic SET domain and resulting in the absence of Ezh2 protein(28). Elimination of both maternal and zygotic contribution of Ezh2, by using the germ cell transplantation technique described previously(28, 30), allowed us to study the function of Ezh2 during early development. As previously shown, *MZezh2* mutant embryos display normal body plan formation and a mild phenotype at 24 hpf. They die at 48 hpf, at which point pleiotropic phenotypes are observed, such as smaller eyes, smaller brain, blood coagulation, and absence of pectoral fins (Figure. 1A). Western Blot analysis at 3.3 hpf and 24 hpf confirmed the absence of both maternal and zygotic Ezh2 in these mutants, respectively (Figure 1B).

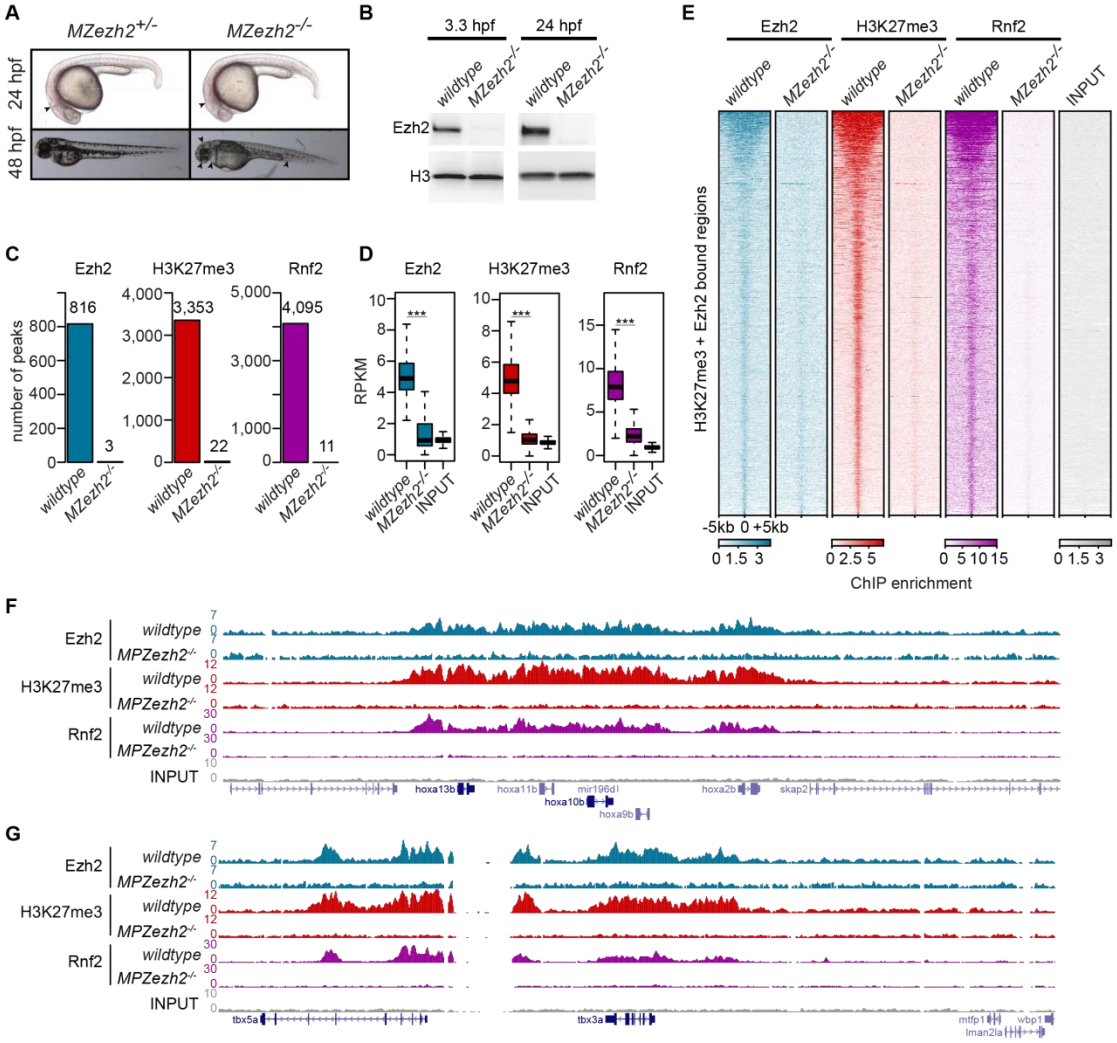

Rougeot_Fig. 1

Figure 1. *MZezh2* mutant (*MZezh2*$^{-/-}$) embryos lack Ezh2, H3K27me3, and Rnf2 binding to the chromatin. (**A**) *MZezh2*$^{+/-}$ (developing as wildtype embryos) and *MZezh2*$^{-/-}$ embryos at 24 and 48 hpf. At 24 hpf, *MZezh2*$^{-/-}$ embryos lack a clear mid-hindbrain boundary compared to heterozygous embryos (arrow head). At 48 hpf, *MZezh2*$^{-/-}$ embryos showed pleiotropic phenotypes compared to heterozygous embryos, such as small eyes, small brain, heart edema, and blood accumulation in the blood island (arrow heads). (**B**) Western blot analysis of Ezh2 at 3.3 hpf and 24 hpf of wildtype and *MZezh2*$^{-/-}$ embryos. Histone H3 was used as a loading control. (**C**) Number of peaks called after Ezh2, H3K27me3, and Rnf2 ChIP-seq of wildtype and *MZezh2*$^{-/-}$ embryos at 24hpf. Each peak set was obtained by the intersection of two independent biological replicates, with the exception of Rnf2

(one replicate). (**D**) Box plots of Ezh2, H3K27me3, and Rnf2 RPKM-normalized coverage after respective ChIP-seq in wildtype and in *MZezh2*$^{-/-}$ embryos at 24 hpf. The input control shown was obtained from wildtype embryos at 24 hpf. Coverages were calculated based on positions of peaks detected in wildtype embryos. t-test: *** *P*-value < 0.001. (**E**) Heatmaps for Ezh2, H3K27me3, and Rnf2 RPKM-normalized coverage after ChIP-seq in 24 hpf wildtype and *MZezh2*$^{-/-}$ embryos. Windows of 10 kb regions for all H3K27me3 o Ezh2 peaks in 24 hpf wildtype embryos are shown. The input track obtained from 24 hpf wildtype embryos was used as control. (**F, G**) UCSC browser snapshot depicting the loss of Ezh2, H3K27me3, and Rnf2 after ChIP-seq in 24 hpf *MZezh2*$^{-/-}$ embryos compared to wildtype embryos for (**F**) the *hoxab* gene cluster and (**G**) *tbx5a*. Colors represent ChIP-seq for different proteins with blue: Ezh2, red: H3K27me3, purple: Rnf2, and grey: Input control.

To further confirm the absence of Ezh2 in *MZezh2* mutants and assess its effect on H3K27me3 deposition, we performed ChIP-sequencing (ChIP-seq) for Ezh2 and H3K27me3 at 24 hpf in both wildtype and *MZezh2* mutant embryos. ChIP-seq analyses for Ezh2 and H3K27me3 revealed 816 and 3,353 peaks in wildtype embryos, respectively (Figure 1C,D, Supplementary Table 1). Although the number of peaks differed between the two proteins, their binding profiles greatly overlap (Figure 1C). Quantification showed that 84.6% of Ezh2 peaks also contain H3K27me3 (Supplementary Figure 1A). Known PcG target genes such as the *hoxab* gene cluster, *tbx* genes, and *gsc* presented similar binding profiles for Ezh2 as for H3K27me3 (Figure 1F,G, Supplementary Figure 1B), whereas the ubiquitously expressed genes *eif1ad* and *tbp* showed absence of Ezh2 and H3K27me3 (Supplementary Figure 1B).

In *MZezh2* mutant embryos, the binding of Ezh2 and H3K27me3, as detected by ChIP-seq, was virtually absent, with 3 and 22 peaks detected for Ezh2 and H3K27me3, respectively (Figure 1C). Manual inspection of these remaining peaks revealed that they are present in gene deserts and low complexity regions and are probably artefacts (Supplementary Figure 1C). Ezh2 and H3K27me3

coverage was reduced to background levels in *MZezh2* mutants compared to wildtype (Figure 1C). Finally, the *hoxab* gene cluster*, tbx3a, tbx5a*, *gsc,* and *isl1* loci, targeted by PcG repression in wildtypes, also showed a complete absence of Ezh2 and H3K27me3 binding in *MZezh2* mutants (Figure 1F,G, Supplementary Figure 1B).

Altogether, these results demonstrate that the absence of maternal and zygotic Ezh2 results in a complete absence of Ezh2 and H3K27me3 from chromatin.

Loss of PRC2-mediated repression results in loss of PRC1 recruitment during early development

It is postulated that PRC1 is recruited to chromatin by PRC2-deposited H3K27me3 but can also have a function independent of PRC2(12-14). As both Ezh2 and H3K27me3 are absent from *MZezh2* mutant embryos, we investigated whether PRC1 is still recruited to chromatin in these mutants. In zebrafish, Rnf2 is the only catalytic subunit of PRC1(31). ChIP-seq for Rnf2 in wildtype embryos at 24 hpf reveals 4,095 peaks (Figure 1C, Supplementary Table 1) which are present at Ezh2 and H3K27me3 positive regions (Figure 1E). We found that 84.9% of Ezh2 peaks were also positive for Rnf2 in wildtype embryos (Supplementary Figure 1A).

In *MZezh2* mutant embryos, only 11 binding sites could be detected for Rnf2 (Figure 1C) and Rnf2 average binding (RPKM) was reduced to background level, as observed for Ezh2 and H3K27me3 binding (Figure 1C,E). This loss of Rnf2 was observed at both gene clusters such as *hoxab* (Figure 1F) and individual transcription factors such as *tbx3a*, *tbx5a*, and *gsc* (Figure 1G, Supplementary Figure 1B). As for Ezh2 and H3K27me3, Rnf2 remaining peaks in *MZezh2* mutant embryos were detected in intergenic regions with repeat sequences and are probably artefacts (Supplementary Figure 1C).

Thus, the loss of PRC2 binding and H3K27me3 deposition in *MZezh2* mutant embryos is associated with a complete loss of Rnf2 on the chromatin.

166

167 **Loss of H3K27me3 in *MZezh2* mutant embryos induces gene specific gain of H3K4me3**

168 As PcG and TrxG complexes are known to have an antagonistic effect on gene expression(32), we
169 investigated whether the loss of H3K27me3 in *MZezh2* mutant embryos changed the deposition
170 H3K4me3, a mark associated with gene activation.

171 To this aim, we performed ChIP-seq for H3K4me3 in both wildtype and *MZezh2* mutant embryos at
172 24 hpf. In total, 11,979 H3K4me3 peaks were detected in wildtype embryos, and 13,401 in *MZezh2*
173 mutants (Figure 2A, Supplementary Table 1). A majority of 11,710 peaks were shared between
174 wildtype and *MZezh2* mutant embryos, whereas 1,691 were specific for *MZezh2* mutants and 269
175 peaks for wildtype embryos (Figure 2A,B). Comparison of the RPKM-normalized H3K4me3 binding
176 levels between *MZezh2* mutant and wildtype embryos showed an overall increase in H3K4me3
177 enrichment upon loss of Ezh2 on the peak locations shared among them (Figure 2B,C). The wildtype
178 specific peak locations presented no difference in RPKM coverage between wildtype and *MZezh2*
179 mutant embryos (Figure 2B). Detection of these wildtype-specific peaks could therefore be explained
180 by the limitation of the peak detection algorithm in accurately identifying low enriched regions,
181 rather than being true wildtype-specific peaks. In contrast, in *MZezh2* mutant embryos, mutant-
182 specific peak locations showed a significant increase in H3K4me3 enrichment level compared to
183 wildtype embryos (Figure 2B). Finally, the binding intensity on the mutant specific H3K4me3 peak
184 locations remained relatively low in *MZezh2* mutant embryos and never reached the enrichment
185 level detected on the H3K4me3 peak locations shared by wildtype and *MZezh2* mutants (Figure
186 2B,C).

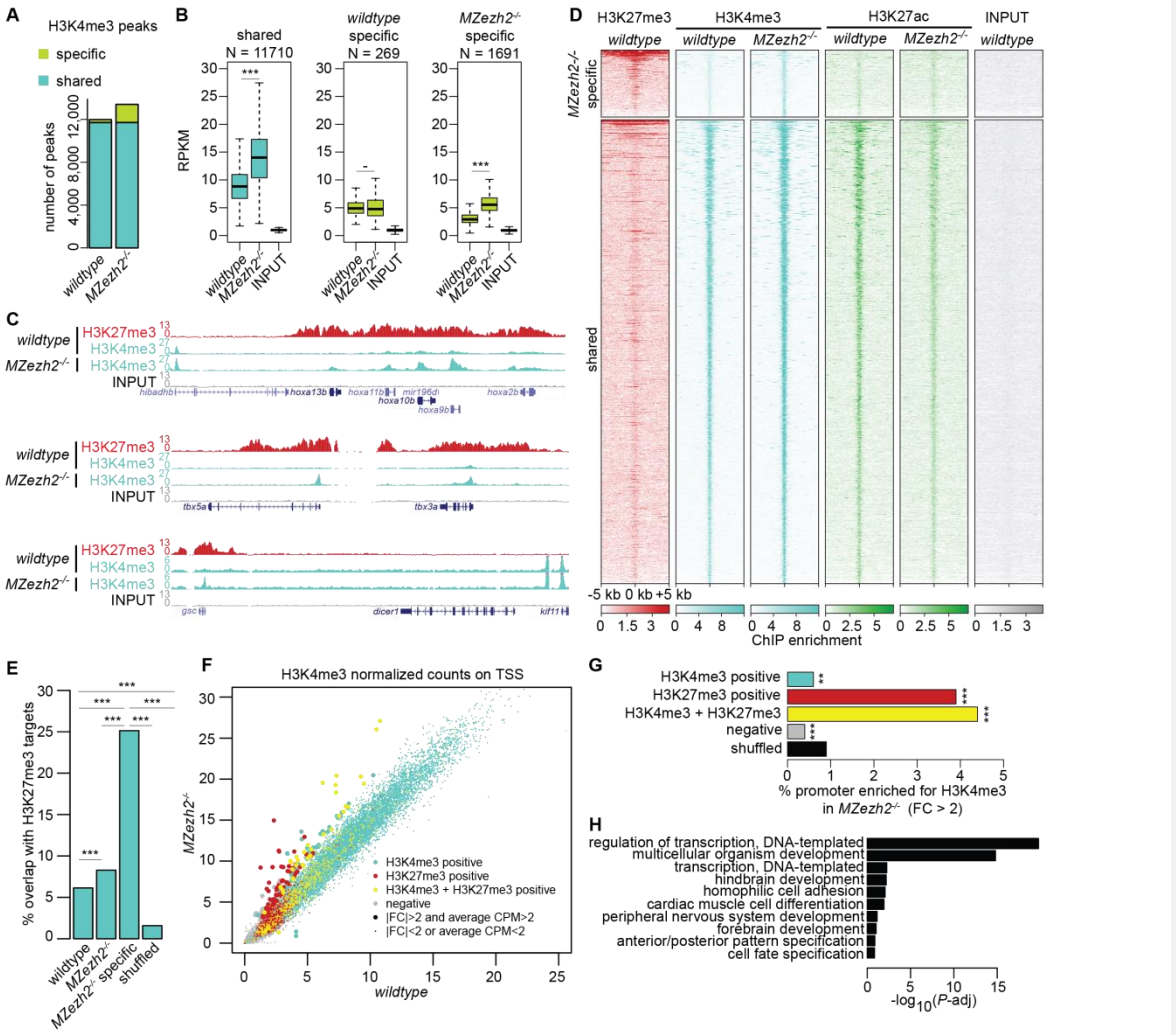

Rougeot_Fig. 2

Figure 2. *MZezh2* mutant (*MZezh2*$^{-/-}$) embryos show an increase in H3K4me3 preferentially on H3K27me3 targets. (**A**) Number of peaks called after H3K4me3 ChIP-seq in wildtype and *MZezh2*$^{-/-}$ embryos at 24 hpf. Turquoise and green represent peaks shared by the two conditions and peaks specific for one condition, respectively. (**B**) Box plots of H3K4me3 RPKM-normalized coverage after ChIP-seq in wildtype and in *MZezh2*$^{-/-}$ embryos at 24 hpf. Colors are similar to (**A**). t-test: *** *P*-value < 0.001. (**C**) UCSC browser snapshots of three genomic loci in wildtype and *MZezh2*$^{-/-}$ embryos at 24 hpf. Red, turquoise, and grey represent ChIP-seq for H3K27me3, H3K4me3, and Input control, respectively. (**D**) Heatmaps of RPKM-normalized coverage after ChIP-seq for H3K27me3 in wildtype embryos and H3K4me3 and H3K27ac in wildtype and *MZezh2*$^{-/-}$ embryos at 24 hpf. Heatmaps display

MZezh2$^{-/-}$ specific peaks and peaks shared by both wildtype and *MZezh2*$^{-/-}$ embryos. The input track obtained from 24 hpf wildtype embryos was used as control. Red, turquoise, green, and grey represent ChIP-seq for H3K27me3, H3K4me3, H3K27ac, and Input control, respectively. (**E**) Percentage of H3K4me3 peaks (+/- 2kb window) showing an overlap with H3K27me3 enriched peaks in 24 hpf wildtype embryos. Selected peak sets are peaks detected at 24 hpf in wildtype embryos, in *MZezh2*$^{-/-}$ embryos, specifically in *MZezh2* mutant embryos (*MZezh2*$^{-/-}$ specific), and a random set of 13,626 peaks as control (shuffled). Bonferroni-corrected χ^2: *** *P*-value < 0.001. (**F**) Scatter plot showing H3K4me3 Count Per Million (CPM) on all transcriptional start sites (TSS) in *MZezh2*$^{-/-}$ embryos as a function of H3K4me3 CPM in wildtype embryos at 24 hpf. Turquoise, red, yellow, and grey dots represent a +/- 2 kb window around TSS positive for H3K4me4, positive for H3K27me3, double positive for H3K4me3 and H3K27me3, and double negative within in 24 hpf wildtype, respectively. (**G**) Percentage of TSS positive for H3K4me3 in *MZezh2*$^{-/-}$ embryos compared to wildtype ($|FC| \geq 2$ and average CPM ≥ 2). TSS sets and colors are identical to (**F**). χ^2: *** *P*-value < 0.001, ** *P*-value < 0.01. (**H**) Gene Ontology analysis of the closest genes restricted two 2kb upstream or downstream from *MZezh2*$^{-/-}$ specific H3K4me3 peaks.

We next assessed if the H3K4me3 peaks gained upon loss of Ezh2 correlated with the presence of H3K27me3 in wildtype embryos. In wildtype embryos, 6.1% of H3K4me3 peaks were also covered by H3K27me3, which is more than expected by random chance (*P*-value < 0.001). In *MZezh2* mutant embryos, a significant increase to 8.3% of the H3K4me3 peaks was found on regions positive for H3K27me3 in wildtypes embryos (*P*-value < 0.001). This enrichment was even higher when taking into account only the *MZezh2* mutant specific H3K4me3 peaks (25.1% with *P*-value < 0.001) (Figure 2D,E). This result shows that the regions positive for H3K27me3 in wildtype are more susceptible to gain H3K4me3 upon loss of H3K27me3.

Next, we determined if the epigenetic landscape at the transcription start sites (TSS) in wildtype embryos had an influence on the ability to gain of H3K4me3 upon loss of Ezh2. We classified all the TSS from the zebrafish in four categories according to our ChIP-seq data in wildtype embryos: active TSS positive for H3K4me3, repressed TSS positive for H3K27me3, TSS positive for both marks, and TSS negative for both marks. Comparison of the level of H3K4me3 binding in *MZezh2* mutant and wildtype embryos on these TSS revealed that 3.9% (*P*-value < 0.001) of the H3K27me3 positive and 4.4% (*P*-value < 0.001) of the H3K4me3/H3K27me3 double positive TSS were enriched (Fold Change: FC ≥ 2) for H3K4me3 in *MZezh2* mutant embryos compared with random TSS (0.9%). TSS positive for only H3K4me3 or negative for both H3K27me3 and H3K4me3 were less likely to show an increase in H3K4me3 binding in *MZezh2* mutant embryos compared with random TSS (0.6%, *P*-value < 0.01 and 0.4%, *P*-value < 0.001 respectively) (Figure 2F,G).

To find all the potential direct targets of PcG-mediated repression gaining H3K4me3 in absence of Ezh2, we searched for the closest genes of the H3K4me3 mutant-specific peaks, which had an H3K27me3 peak in wildtype embryos, and identified 463 genes. Gene ontology analysis revealed that these genes were mainly involved in transcriptional regulation and organismal development (Figure 2H). Among these 463 identified genes, 143 encode for transcription factors, among which were members of the *hox*, *tbx*, *sox*, and *pax* gene families, known targets of PcG complexes.

During development, gene transcription is also controlled by enhancer activation(33). H3K27me3 and H3K27ac are known to have an opposite effect on enhancer activation, the former being associated to poised enhancers and the latter to active enhancers(34). We studied the binding of H3K27ac in 24 hpf embryos lacking H3K27me3. Unlike H3K4me3, the number of peaks enriched for H3K27ac decreased by more than a half in *MZezh2* mutants compared with wildtype (4,155 and 8,952 peaks detected, respectively) (Supplementary Figure 2A, Supplementary Table 1). This loss of H3K27ac was associated with a decrease in coverage intensity (Supplementary Figure 2B).

These results suggest that loss of PcG-mediated repression has a specific effect rather than a general impact on deposition of activating epigenetic marks.

Epigenetic changes in *MZezh2* mutant embryos induce upregulation of transcription factors

As *MZezh2* mutant embryos show a complete lack of the H3K27me3 repressive mark and a selective increase in H3K4me3 activating mark on genes coding for transcription factors, we investigated the effect of loss of Ezh2 on the transcriptome by RNA-sequencing (RNA-seq) of wildtypes and *MZezh2* mutants at 24 hpf. Differential gene expression analysis between the two conditions revealed a limited effect on the transcriptome upon the loss of Ezh2. Only 60 genes were detected to be significantly upregulated ($log_2FC \geq 1$ and *P*-adj < 0.05) and 28 genes downregulated ($log_2FC \leq -1$ and *P*-adj < 0.05) in *MZezh2* mutants (Figure 3A). When inspecting the upregulated genes, we found 60% of the upregulated genes (compared to 9.3% in all genes, *P*-value < 0.001) to be targeted by H3K27me3 in wildtype embryos (Figure 3B,C). On the other hand, the upregulated genes were less likely to be targeted by H3K4me3 in wildtype embryos compared to all zebrafish genes (21.7% compared to 47.8%, *P*-value < 0.001), yet gained significant binding of H3K4me3 in *MZezh2* mutant embryos (23.3% compared to 5.3%, *P*-value < 0.001, Figure 3B,C). No gain of H3K4me3 was detected on genes downregulated in *MZezh2* mutants (Figure 3B,C).

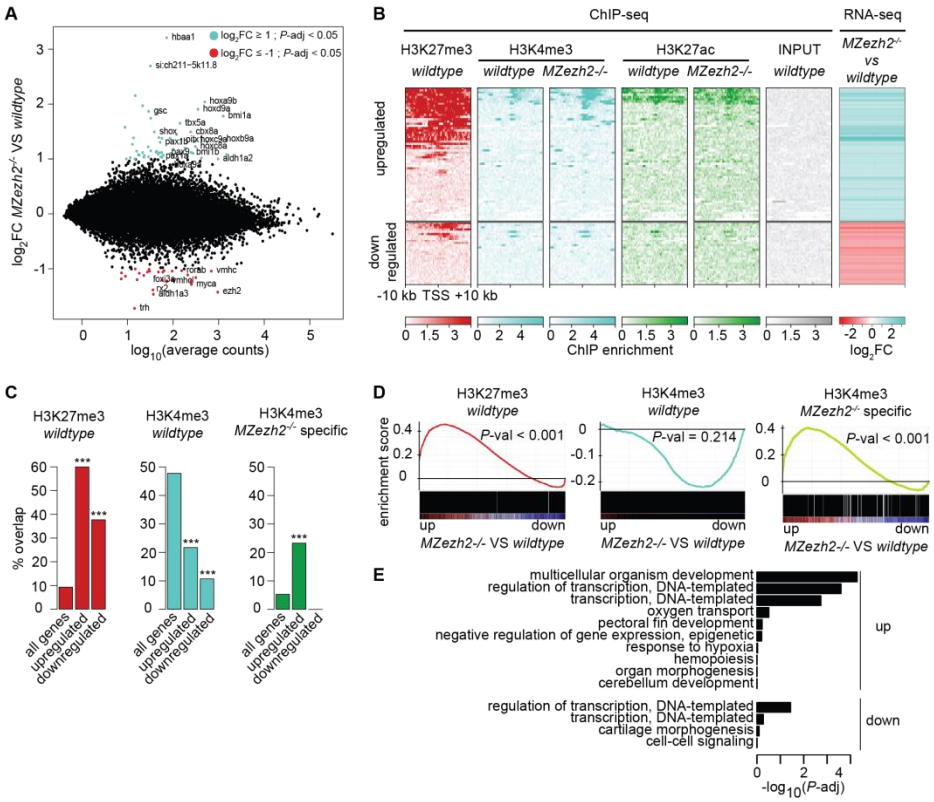

Rougeot_Fig. 3

Figure 3. Loss of maternal zygotic *ezh2* results in overexpression of specific developmental genes. (**A**) MA-plot showing the fold change (log_2-transformed) between gene expression in 24 hpf *MZezh2* mutant (*MZezh2*$^{-/-}$) and wildtype embryos as a function of the normalized average count between the two conditions (log_{10}-transformed) as calculated with DEseq2. Turquoise: $log_2FC \geq 1$ and *P*-adj < 0.05, red: $log_2FC \leq -1$ and *P*-adj < 0.05. (**B**) Heatmaps of RPKM-normalized coverage after ChIP-seq for H3K27me3 in wildtype embryos and H3K4me3 and H3K27ac in wildtype and *MZezh2*$^{-/-}$ embryos at 24 hpf. Heatmaps display 20 kb regions around TSS from genes detected upregulated or downregulated in *MZezh2*$^{-/-}$ embryos compared to wildtype embryos at 24 hpf. The input track obtained from 24 hpf wildtype embryos was used as control. Most right column represents differential gene expression analysis in *MZezh2*$^{-/-}$ compared to wildtype embryos at 24 hpf. Colors represent ChIP-seq for different proteins with red: H3K27me3, turquoise: H3K4me3, green: H3K27ac, and grey: Input control. For RNA-seq, turquoise represent overexpressed genes and red downregulated genes. (**C**) Percentage of TSS (+/- 2kb window) showing an overlap with H3K27me3

(red, left) or H3K4me3 (turquoise, center) in wildtype embryos and with *MZezh2*$^{-/-}$ specific H3K4me3 (green, right) at 24 hpf. Selected TSS sets are all TSS from annotation, TSS from genes upregulated in *MZezh2*$^{-/-}$ embryos, and TSS from genes downregulated in *MZezh2*$^{-/-}$ embryos at 24 hpf. χ^2: *** *P*-value < 0.001. (**D**) Gene Set Enrichment Analysis (GSEA) plots of gene expression changes in *MZezh2*$^{-/-}$ embryos compared to wildtype embryos at 24 hpf. Gene sets used for the analyses are H3K27me3 positive genes in wildtype embryos (red, left), H3K4me3 positive genes in wildtype embryos (turquoise, center), and H3K4me3 positive genes in *MZezh2*$^{-/-}$ embryos specifically (green, right) at 24 hpf. (**E**) Gene Ontology of biological processes analysis of genes upregulated or downregulated in *MZezh2*$^{-/-}$ embryos compared to wildtype embryos at 24 hpf.

As a complement, we studied the relation between changes in transcriptome and epigenome by performing Gene Set Enrichment Analysis (GSEA)(35, 36). This analysis revealed that the genes upregulated in *MZezh2* mutants showed enrichment for the set of genes occupied by H3K27me3 in wildtype embryos (n=2336, Fig 3d, left panel). The set of genes positive for H3K4me3 in wildtype embryos (n=11979) showed no enrichment for neither upregulated nor downregulated genes in *MZezh2* mutants (Figure 3D, middle panel). The genes with higher expression in *MZezh2* mutants showed a clear association with the presence of *MZezh2* mutant specific H3K4me3 peaks (n=1317, Figure 3D, right panel). Thus, through the GSEA, we can confirm the association between the loss of H3K27me3 repressive chromatin and the gain of new H3K4me3 positive chromatin on specific loci with the gain in gene expression in *MZezh2* mutant embryos at 24 hpf.

GO analysis of the deregulated genes in *MZezh2* mutants revealed enrichment in biological processes of regulation of transcription and development (Figure 3E), a majority of these genes encoding for transcription factors. Anatomical terms associated with the deregulated genes indicated that these genes were expressed in organs showing strong phenotypes in *MZezh2* mutant embryos, such as fin bud, retina, and heart tube (Supplementary Figure 3A).

Deregulations in epigenome and transcriptome are linked to changes in protein expression in *MZezh2* mutant embryos

We next performed proteomic analysis of the *MZezh2* mutant embryos and compared the result with wildtype embryos at 24 hpf. Differential analysis revealed 111 upregulated ($log_2FC \geq 1.5$ and *P-adj* < 0.05) and 110 downregulated ($log_2FC \leq -1.5$ and *P-adj* < 0.05) proteins (Figure 4A, Supplementary Table 1). After ranking the proteins based on their difference in expression between the two conditions, we explored those differences in the context of different epigenetic marks and changes in the transcriptome by GSEA. Results showed that upregulated proteins were enriched in H3K27me3 targets in wildtypes and presented mutant-specific H3K4me3 peaks in *MZezh2* mutant embryos (Figure 4B). Upregulation and downregulation of protein expression also correlated with deregulation of gene expression in transcriptome (Figure 4C). For example, *hoxa9b* was one of the top overexpressed targets in both the transcriptome and proteome analyses (Figure 3A, Figure 4A, Supplementary Table 1).

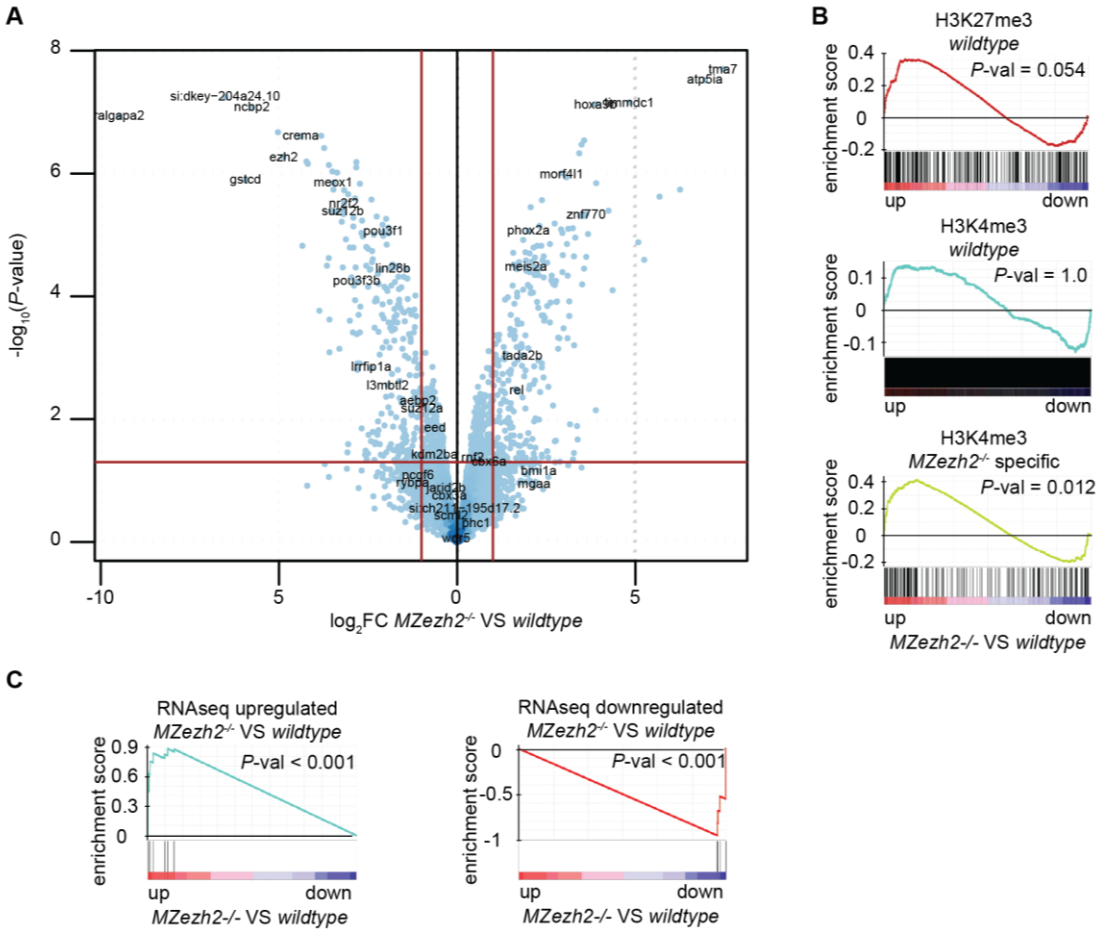

Rougeot_Fig4

Figure 4. Chromatin and transcriptome changes are translated at the protein level. (**A**) Volcano plot showing the *P*-value (-$\log_{10}$-transformed) as a function of the fold-change ($\log_2$-transformed) between protein expression level in *MZezh2* mutant (*MZezh2*$^{-/-}$) compared to wildtype embryos at 24 hpf. (**B**) GSEA plots of protein expression changes in *MZezh2*$^{-/-}$ embryos compared to wildtype embryos at 24 hpf. Gene sets used for the analyses are H3K27me3 positive genes in wildtype embryos (red, top), H3K4me3 positive genes in wildtype embryos (turquoise, middle), and *MZezh2*$^{-/-}$ specific H3K4me3 positive genes (green, bottom) at 24 hpf. (**C**) GSEA plots of protein expression changes in *MZezh2*$^{-/-}$ embryos compared to wildtype embryos at 24 hpf. Gene sets used for the analyses are genes found upregulated (turquoise, left) and genes found downregulated (red, right) in *MZezh2*$^{-/-}$ compared to wildtype embryos at 24 hpf in our RNA-seq experiments.

Furthermore, in addition to Ezh2, Suz12b was found to be downregulated in *MZezh2* mutant embryos (Figure 4A). Other PRC2 subunits were either not detected or (not significantly) downregulated. Subunits of the canonical PRC1 complex were mostly overexpressed, although not significant (Supplementary Figure 3B).

The low number of deregulated genes detected by both transcriptomic and proteomic analyses suggests that changes in expression could be either global and low in intensity or limited to specific cell types or tissues. To test these hypotheses, we carried out a spatial expression analysis on selected target genes.

Loss of *ezh2* results in expression of *hox* genes outside their normal expression domains

To start with, we focused on expression of different genes from the *hox* gene family. These genes are known targets of Polycomb-mediated repression(37) and some of them have been previously shown to be deregulated in *MZezh2* mutant embryos(28). Every *hox* gene has an expression pattern that is restricted along the anterior-posterior axis(38). To obtain spatially resolved data along the anterior-posterior axis, we performed RT-qPCR on the anterior half and the posterior half of 24 hpf wildtype and *MZezh2* mutant embryos. We then compared the normalized relative expression levels between the different halves of the *MZezh2* mutant and wildtype embryos. The tested *hox* genes were selected based on their domain of expression along the anterior-posterior axis (Figure 5A-D). The *hoxa9a* gene, whose expression extends to anterior, until slightly outside the posterior half of the embryos, showed, as expected, a higher expression in the posterior part than in the anterior part in wildtype embryos (Figure 5A). In *MZezh2* mutants, *hoxa9a* was overexpressed in the anterior compartment compared with wildtype embryos, reaching levels similar to those observed in the posterior part of wildtype embryos. No significant differences were detected in the level of

350 expression when comparing the posterior compartment of *MZezh2* mutant and wildtype embryos
351 (Figure 5A). Similar results were obtained for *hoxa9b*, where overexpression was detected in the
352 anterior compartment of *MZezh2* mutant embryos compared to the anterior compartment of
353 wildtype embryos (Figure 5B). The *hoxa11b* and *hoxa13b* genes, which are expressed primarily
354 posterior, showed, as expected, higher expression in the posterior half of the wildtype embryos
355 compared to the anterior half (Figure 5C,D). In the *MZezh2* mutant embryos, both *hox* genes were
356 upregulated in the anterior half of the *MZezh2* mutant embryos compared to wildtypes (Figure 5C,D)
357 but their expression level remained lower than in the posterior half of the wildtype embryos (Figure
358 5C,D).

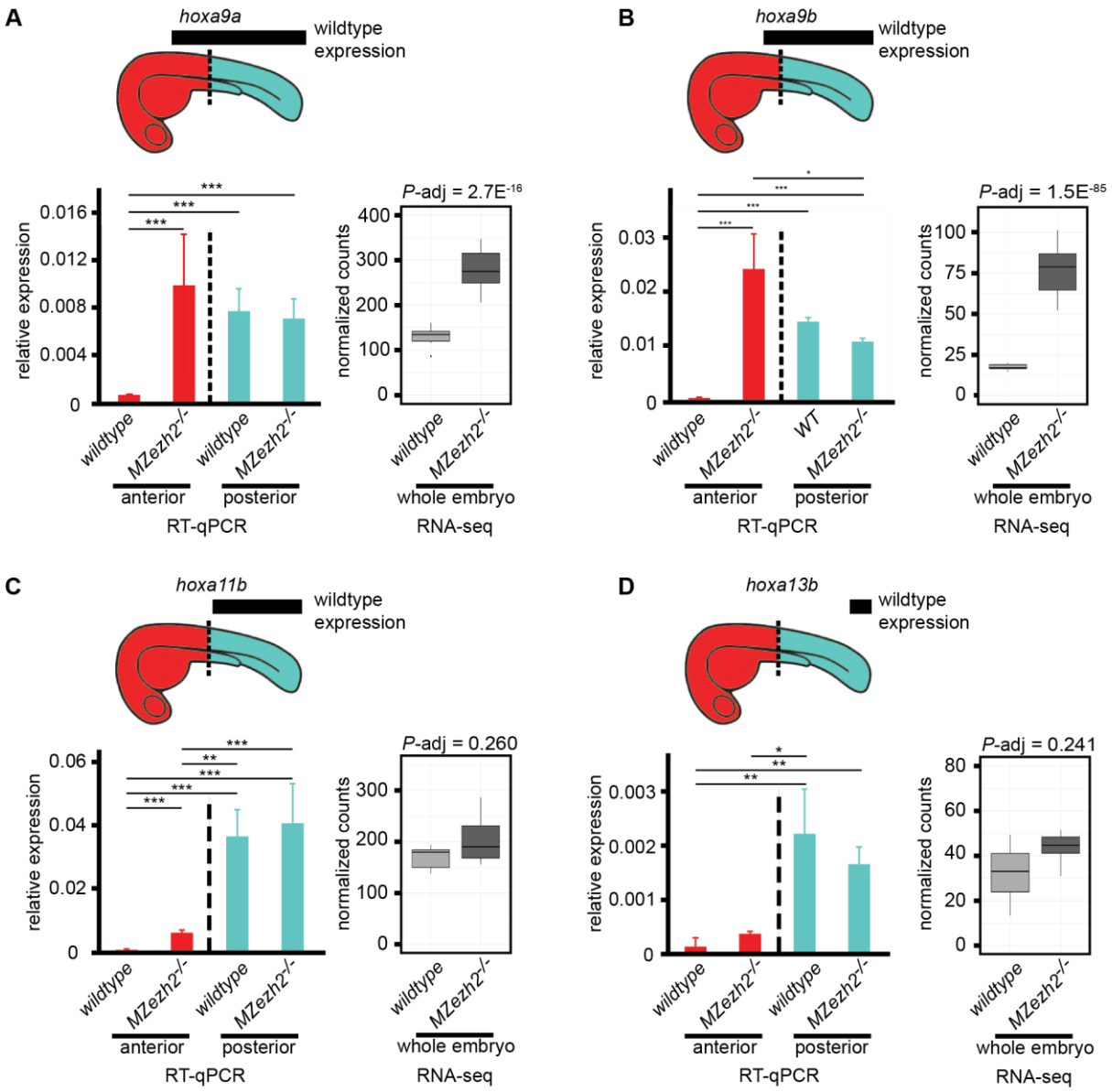

Rougeot_Fig. 5

Figure 5. Loss of maternal and zygotic *ezh2* results in ectopic expression of *hox* genes. (**a**, **b**, **c**, **d**) Expression analysis of (**A**) *hoxa9a,* (**B**) *hoxa9b*, (**C**) *hoxa11b,* and (**D**) *hoxa13b* at 24 hpf. Bar plots on the left side of each panel represent relative expression of indicated *hox* genes in the anterior half (red) and posterior half (turquoise) of wildtype and *MZezh2* mutant (*MZezh2*$^{-/-}$) embryos. Boxplots on the right side of each panel represent normalized counts from RNA-seq experiments in *MZezh2*$^{-/-}$ and wildtype whole embryo lysates at 24 hpf. Above is a schematic representation of 1 dpf embryos. Black boxes represent the expression domains of the *hox* genes in wildtype embryos based on

published data(39). Dashed lines represent the demarcation between anterior (red) and posterior (turquoise) parts of the embryo used for RT-qPCR analysis. For RT-qPCR, relative expression was calculated based on expression of housekeeping gene *actb1*. Error bars represent standard deviations. Relative expression was compared between anterior or posterior parts in *MZezh2*$^{-/-}$ and wildtype embryos (one-way ANOVA with post-tests, *** *P*-value < 0.001, ** *P*-value < 0.01, * *P*-value < 0.05). For RNA-seq, adjusted *P*-values were extracted from Differential Expression analysis with DEseq2.

These comparative analyses of anterior and posterior parts of the embryo suggest that, upon loss of Ezh2, *hox* genes show an ectopic anterior expression while keeping wildtype expression levels in their normal expression domains.

Different transcription factors show various profiles of deregulation in the absence of Ezh2

To further pursue our investigation on the changes in gene expression patterns in absence of Ezh2, we performed *in situ* hybridization (ISH) on members from the *tbx* gene family of transcription factors. The *tbx2a*, *tbx2b*, *tbx3a*, and *tbx5a* genes have partial overlapping expression patterns in wildtype embryos, but also display gene specific expression domains (Figure 6A). At 24 hpf, these *tbx* gene family members are expressed in the dorsal region of the retina, in the heart, and the pectoral fins(40, 41). In addition, the genes *tbx2a*, *tbx2b*, and *tbx3a* are expressed in the otic vesicle. The genes *tbx2b* and *tbx3a* are expressed in different ganglions and neurons in anterior and posterior regions of wildtype embryos(40). Finally, expression of *tbx2b* can also be detected in part of pharyngeal arches 3-7 and the distal region of the pronephros and *tbx3a* expression can be detected in the brachial arches(39). This spatial prevalence of *tbx* gene expression in the anterior half of the

390 embryo was also detected by RT-qPCR at 24 hpf, where *tbx2a*, *tbx2b* and *tbx5a* expression was

391 significantly higher in the anterior than in the posterior part of wildtype embryos (Figure 6B).

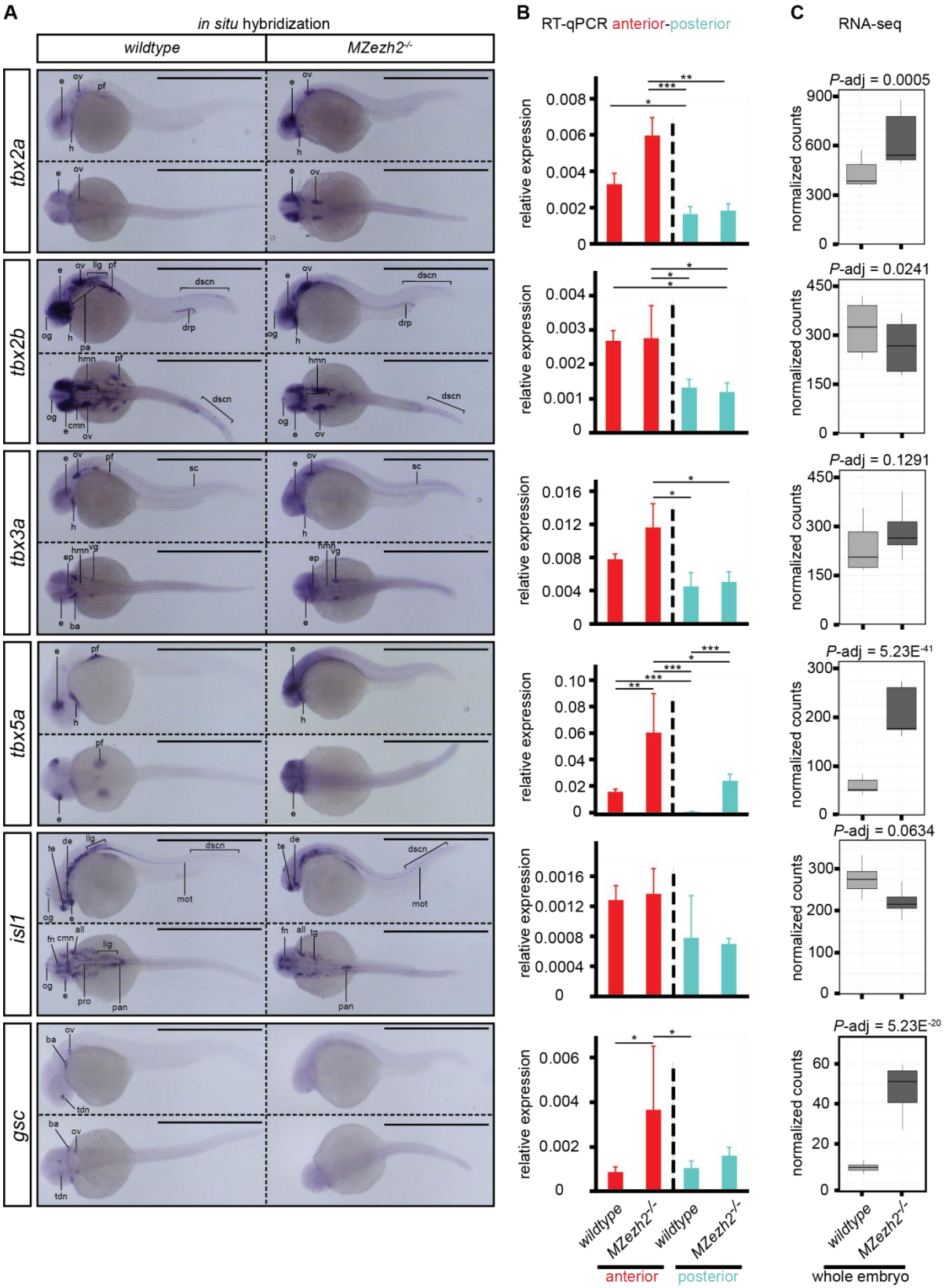

392 Rougeot_Fig. 6

Figure 6. Transcription factor expression is spatially deregulated in *MZezh2* mutant (*MZezh2*$^{-/-}$) embryos. (**A**, **B**, **C**) Spatial expression analysis by (**A**) *in situ* hybridization (ISH), (**B**) RT-qPCR on anterior half and posterior half, and (**C**) RNA-seq results of transcription factors *tbx2a, tbx2b, tbx3a*, *tbx5a*, *isl1*, and *gsc* in 24 hpf embryos. In ISH, scale bars represent 1 mm. For RT-qPCR, relative expression was calculated based on expression of housekeeping gene *actb1*. Error bars represent standard deviations. Relative expression was compared between anterior (red) or posterior (turquoise) parts in *MZezh2*$^{-/-}$ and wildtype embryos (one-way ANOVA with post-tests, *** *P*-value < 0.001, ** *P*-value < 0.01, * *P*-value < 0.05). Right boxplots represent normalized counts from RNA-seq experiments in whole *MZezh2*$^{-/-}$ and wildtype embryos and adjusted *P*-values were taken from Differential Expression analysis with DEseq2. all: anterior lateral lane ganglion, ba: branchial arch, cmn: cranial motor neurons, de: diencephalon, drp: distal region of the pronephros, dscn: dorsal spinal cord neurons, e: eye, ep: epiphysis, fn: forebrain nuclei, h: heart, hmn: hindbrain motor neurons, llg: lateral lane ganglion, mot: primary motor neurons, og: olfactory ganglion, ov: otic vesicle, pa: pharyngeal arches, pan: pancreas, pf: pectoral fin, pro: pronephros, sc: spinal cord, tdn: telencephalon and diencephalon nuclei, te: telencephalon, vg: ventral ganglion.

ISH for these *tbx genes* on *MZezh2* mutant embryos at 24 hpf suggests ectopic expression of these transcription factors around their normal expression pattern in the eye, the otic vesicle, and the heart, except for *tbx2b* (Figure 6A). This scattering in gene expression was reflected in a trend towards a higher expression in the anterior half of *MZezh2* mutant embryos as detected by RT-qPCR, although only *tbx2a* and *tbx5a* results were significant (Figure 6B). In addition, ISH for *tbx5a*, and to a lesser extent *tbx3a*, showed ubiquitous expression throughout the entire body of *MZezh2* mutants which was not visible in wildtypes (Figure 6A). RT-qPCR results confirmed increased expression of *tbx5a* in both the anterior and posterior half of the *MZezh2* mutant embryos (Figure 6B).

Beside the observed ectopic expression, all tested *tbx* genes showed absence of expression in specific structures upon Ezh2 loss. For example, in *MZezh2* mutant embryos, all four *tbx* genes showed no expression in the fin bud (Figure 6A). In *MZezh2* mutant embryos, the gene *tbx2b* showed no expression in the pharyngeal arches 3-7 and the lateral line ganglions, and *tbx3a* was not observed in the branchial arches (Fig 6a). This absence of expression was not detected by RT-qPCR (Figure 6B) but a trend toward downregulation for *tbx2b* was observed in RNA-seq results on whole *MZezh2* mutant embryo lysates (Figure 6C).

In addition, we tested transcription factors from other families which were targeted by H3K27me3 in wildtype. The transcription factor *isl1*, expressed in all primary neurons(42), showed a similar absence of expression in the fin bud and the cranial motor neurons in the midbrain (trigeminal, facial and vagal motor neurons), as observed for *tbx2a*. Its expression was also absent in the ventral region of the eye, the facial ganglia, and in the pronephros from *MZezh2* mutant embryos, where it is normally expressed in wildtype embryos(43, 44) (Figure 6A). This loss in expression in *MZezh2* mutant embryos was not detected by RT-qPCR but a clear tendency toward downregulation was detected by RNA-seq (Figure 6B,C). Even more surprising was the expression pattern of *gsc* in the *MZezh2* mutant embryos. Whereas all the wildtype embryos show highly specific expression in the telencephalon and diencephalon nuclei, the branchial arches, and the otic vesicle(39), *gsc* expression was lost and replaced by a weak but ubiquitous expression in *MZezh2* mutant embryos (Figure 6A). This observation was confirmed by RT-qPCR and RNA-seq where upregulation of *gsc* was clearly detected in *MZezh2* mutant embryos (Figure 6B,C).

Taken together, these spatial expression analyses showed that the tested transcription factors are expressed outside their normal wildtype expression boundaries in *MZezh2* mutant embryos at 24 hpf. Furthermore, expression of some of these genes is lost in specific tissues in the *MZezh2* mutant embryos.

Discussion

Here, we showed for the first time the genome-wide binding patterns of Ezh2 and Rnf2, the catalytic subunits of PRC2 and PRC1, respectively, in 24 hpf zebrafish embryos. The overall overlap between the binding patterns of Ezh2, Rnf2, and the PcG related epigenetic mark H3K27me3 suggests that the PcG-mediated gene repression mechanisms(6) are evolutionary conserved in zebrafish development. The complete loss of H3K27me3 in *MZezh2* mutant embryos reveals that Ezh2 is the only methyltransferase involved in trimethylation of H3K27 during early zebrafish development. This result was expected as Ezh1, the only other H3K27me3 methyltransferase, is not maternally loaded nor expressed in the zebrafish embryo until at least after 1 dpf(28, 45-47). In addition, proteomics results showed decreased protein expression of most PRC2 subunits. This could indicate a destabilization of PRC2 in absence of the catalytic subunit in *MZezh2* mutant embryos. We could therefore confirm that zebrafish embryos can form a normal body plan in absence of PRC2-mediated gene repression.

The total loss of Rnf2 binding in the *MZezh2* mutants suggests that only the canonical pathway, in which PRC2 is required for PRC1 recruitment, is active during this stage of development. This absence of PRC1 recruitment to the chromatin is not caused by an absence of the complex in the *MZezh2* mutants, since most of the PRC1 subunits were detectable and even upregulated as shown by proteomic analysis. This is in contrast with studies in cultured mouse embryonic stem cells where non-canonical PRC1 complexes were shown to be recruited to developmental regulated genes independently of PRC2(12, 14). This difference could be explained by the complete absence of H3K27me3 since fertilization in *MZezh2* mutant embryos, whereas other studies used conditional knockdown. Therefore, our model suggests that the PRC2-independent recruitment of PRC1 during

466 early development can occur if PRC1 recruitment was first primed by a PRC2-dependent mechanism
467 happening earlier during development.

468 As repressive and activating marks are known to antagonize each other(16), one could expect an
469 increase in the H3K4me3 level deposited by TrxG proteins in absence of H3K27me3 associated with
470 an increase in gene activation. However, the effects on H3K4me3 deposition, gene expression, and
471 protein expression are limited in *MZezh2* mutant embryos at 24 hpf. This observation is in
472 agreement with the near complete absence of phenotype at this developmental time point. Thus, it
473 appears that transcriptional regulation during zebrafish development is largely PRC2-independent
474 until later stages of development, when maintenance of cellular identity is required. These results
475 were unexpected, as PRC2 is described to be essential during mammalian development already
476 during gastrulation(19-21). Exploring distribution of other repressive epigenetic marks in *MZezh2*
477 mutant embryos could reveal compensation mechanisms safeguarding gene repression during early
478 development, as it was previously shown that absence of both DNA methylation and H3K9me3 could
479 influence H3K27me3, and reciprocally(48-50). Possibly, the external development of the zebrafish
480 could also explain this difference in phenotype.

481 Although limited, genes that show a gain in H3K4me3 deposition or in expression upon loss of *ehz2*
482 are mainly transcription factors targeted by H3K27me3 in wildtype embryos. That only a minor
483 fraction of all H3K27me3 target genes gained expression (4.1%) suggests different mechanisms of
484 regulation of PcG target genes. Our hypothesis is that control of gene expression by signaling
485 pathways and transcription factor networks(51) is a robust mechanism and can be maintained until 1
486 dpf in absence of repression by PcG complexes. At 1 dpf, in absence of PcG-mediated repression, the
487 first derepressed genes will be the genes subjected to the most fine-tuned transcriptional control,
488 such as genes controlled by precise morphogen gradients. For example, it was shown that PRC2
489 attenuates expression of genes controlled by retinoic acid signaling(52, 53). In vertebrates, and most
490 particularly zebrafish, retinoic acid signaling is responsible for induction of formation of, among

others, the forelimb field(54, 55), dorsoventral patterning of eyes(56, 57), hindbrain patterning(58), *hox* gene expression(59), and the development of other organs(60). All these processes are affected in *MZezh2* mutant embryos at 24 hpf and onwards and, therefore, could be explained by a defect in the response to retinoic acid signaling.

Spatial analysis of gene expression revealed different effects on gene expression patterns caused by loss of Ezh2, which could not be detected by RNA-seq on whole embryo lysates. Anterior-posterior specific RT-qPCR showed that *hox* genes become abnormally expressed in the anterior half of the *MZezh2* mutant embryos; whereas expression levels in the posterior half remained unchanged. These results are in agreement with previous studies showing ectopic expression of *hox* genes in PRC1 and PRC2 zebrafish mutants(28, 61). Other transcription factors, such as the *tbx* gene family members, showed more diverse patterns of deregulation compared to *hox* genes. ISH and RT-qPCR showed that, among the *tbx* genes examined, some were overexpressed outside their normal expression domains (*tbx2a, tbx3a, and tbx5a*), whereas others were also ubiquitously upregulated (*tbx3a* and *tbx5a*). The case of eye patterning is a good example of the defect in control of gene expression pattern in *MZezh2* mutant embryos. In wildtype embryos, at 24 hpf, *tbx* genes are expressed in the dorsal part of the eye whereas *isl1* is expressed in the ventral part. Upon loss of Ezh2, our ISH results showed that the expression of the *tbx* genes expands to the whole eye whereas *isl1* disappears from the ventral region. We concluded that Polycomb-mediated repression is therefore responsible for maintenance of expression domains rather than control of expression level.

Expression analysis by ISH for *tbx* and *hox* genes as well as for *isl1* also showed loss of expression in specific structures in *MZezh2* mutant embryos. We reasoned that the absence of expression of *hox* and *tbx* genes in the fin bud could be a secondary effect due to the absence of this structure in *MZezh2* mutants(28). The same phenomenon could explain the lack of detection of *tbx2b* and *isl1* in pharyngeal arches, pronephros, and lateral line ganglions. The case of *gsc* expression is more

striking, as its normal expression pattern is totally abolished and replaced by a ubiquitous expression pattern. The *gsc* gene is known to be expressed in the Spemann organizer during gastrulation and therefore all cells will transiently express *gsc* when undergoing gastrulation(62, 63). In absence of Ezh2, *gsc* expression could remain active in all cells after leaving the Spemann organizer, leading to a ubiquitous expression pattern and impaired tissue specific expression in 24 hpf *MZezh2* mutant embryos.

To conclude, our results show that early embryonic development, including germ layer formation and cell fate specification, is independent of PcG-mediated gene repression until axis are formed and organs specified. PcG-mediated gene repression is then required to control precise spatial restricted expression of specific transcription factors. We hypothesize that subtle changes in expression of these master gene regulators subsequently will lead to progressive and accumulating changes in gene network regulation and result in loss of tissue identity maintenance. Our results constitute a major advance in the understanding of the mechanisms of PcG-mediated epigenetic gene regulation during vertebrate development.

Materials and methods

Zebrafish genetics and strains

Zebrafish (*Danio rerio*), were housed according to standard conditions(64) and staged according to Kimmel et al.(65). The *ezh2* nonsense mutant (*hu5670*)(28), *Tg(H2A::GFP)*(66), and *Tg(vas::eGFP)*(67) zebrafish lines have been described before. Genotyping of the *ezh2* allele was performed as previously described(28) with following adaptations: different primer pairs were used for PCR and nested PCR (Supplementary Table S2), of which the restriction profile is shown on Supplementary

539 Figure 1F. All experiments were carried out in accordance with animal welfare laws, guidelines, and
540 policies and were approved by the Radboud University Animal Experiments Committee.
541
542 **Germ cell transplantation**
543 Germ cell transplantation was performed as described previously(28). For all experiments below,
544 *ezh2* germline mutant females were crossed with *ezh2* germline mutant males to obtain 100%
545 *MZezh2* mutant progeny. The germline wild-type sibling males and females obtained during
546 transplantation were used to obtain 100% wildtype progeny with similar genetic background and are
547 referred to as wildtype. The embryos used were all from the first generation after germline
548 transplantation.
549
550 **Western blotting**
551 At 3.3 hpf, 50 embryos were collected, resuspended in in 500 µl ½ Ringer solution (55 mM NaCl, 1.8
552 mM KCl, 1.25 mM $NaHCO_3$) and forced through a 21G needle and a cell strainer in order to remove
553 the chorion and disrupt the yolk. At 24 hpf, 20 embryos were collected and resuspended by
554 thorough pipetting in 500µl ½ Ringer solution in order to disrupt the yolk. The samples of 3.3 and 24
555 hpf were centrifuged for 5 minutes at 3,500 g at 4°C and washed two additional times with 500 µl ½
556 Ringer solution. The embryo pellet was frozen in liquid nitrogen and stored at -80°C. Whole protein
557 extraction was performed by adding 40 µl of RIPA buffer (100 mM Tris-HCl pH 8, 300 mM NaCl, 2%
558 NP-40, 1% Sodium Deoxycholate, 0.2% SDS, 20% glycerol, 1x cOmplete EDTA-free protease inhibitor
559 cocktails from Sigma) and sonication for 2 cycles of 15s ON and 15s OFF on medium power at 4°C on
560 a PicoBioruptor (Diagenode). After 10 minutes incubation at 4°C, embryo lysates were centrifuged
561 for 12 minutes at 16,000 g at 4°C and supernatant was transferred in a new tube. 20 µg protein was
562 mixed with SDS containing sample loading buffer, denaturated at 95°C for 5 minutes and analyzed by
563 Western blot analysis. Antibodies used for immunoblotting are described in Supplementary Table S3
564 HRP-conjugated anti-rabbit secondary antibody was used (Supplementary Table S3) and protein

565 detection was performed with ECL Select Western Blotting Detection Reagent (GE Healthcare,
566 RPN2235) on an ImageQuant LAS 4000 (GE Healthcare).
567
568 **ChIP-sequencing**
569 For chromatin preparation, embryos from a germline mutant or germline wildtype incross were
570 collected at 24 hpf and processed per batches of 300 embryos. Embryos were first dechorionated by
571 pronase (0.6 µg/µl) treatment and then extensively washed with E3 medium. Subsequently, embryos
572 were fixed in 1% PFA (EMS, 15710) for 15 minutes at room temperature and fixation was terminated
573 by adding 0.125M glycine and washed 3 times in cold PBS. Yolk from fixed embryos was disrupted by
574 pipetting the fixed embryos 10 times with a 1 ml tip in 600 µl of ½ Ringer solution (55 mM NaCl, 1.8
575 mM KCl, 1.25 mM $NaHCO_3$) and incubated for 5 minutes at 4°C on a rotating wheel. Embryos were
576 pelleted by centrifuging 30 seconds at 300 g and the supernatant was removed. De-yolked embryos
577 were resuspended in 600 µl sonication buffer (20 mM Tris-HCl pH 7.5, 70 mM KCl, 1 mM EDTA, 10%
578 glycerol, 0.125% NP40, 1x cOmplete EDTA-free protease inhibitor cocktails from Sigma) and
579 homogenized with a Dounce homogenizer (6 strokes with pestle A, followed by 6 strokes with pestle
580 B). Homogenates were sonicated for 6 cycles of 30 seconds ON/30 seconds OFF on a PicoBioruptor
581 (Diagenode), centrifuged for 10 minutes at 16,000 g at 4°C, and the supernatant containing the
582 chromatin was stored at -80°C. 20 µl of the supernatant was subjected to phenol-chloroform
583 extraction and ran on an agarose gel to verify that a proper chromatin size of 200-400 bp was
584 obtained.
585 For ChIP, 100 µl of chromatin preparation (corresponding to 50 embryos) was mixed with 100 µl IP-
586 buffer (50 mM Tris-HCL pH 7.5, 100 mM NaCl, 2 mM EDTA, 1% NP-40, 1x cOmplete EDTA-free
587 protease inhibitor cocktails from Sigma) and antibody (for details on antibodies used see
588 Supplementary Table S3) and incubated overnight at 4°C on a rotating wheel. For
589 immunoprecipitation, 20 µl of protein G magnetic beads (Invitrogen, 1003D) were washed in IP
590 buffer and then incubated with the chromatin mix for 2 hours at 4°C on a rotating wheel. Samples

were washed in 500 µl washing buffer 1 (IP-buffer + 0.1% Sodium Deoxycholate), followed by washing in washing buffer 2 (washing buffer 1 + 400mM NaCl), washing buffer 3 (washing buffer 1 + 250mM LiCl), washing buffer 1 and a final wash in 250 µl of TE buffer. All washes were 5 minutes at 4°C on a rotating wheel. Chromatin was eluted from the beads by incubation in 100 µl of elution buffer (50 mM $NaHCO_3$ pH 8.8, 1% SDS) for 15 minutes at 65°C at 900 rpm in a thermomixer. The supernatant was transferred in a clean 1.5 ml tube. Elution was repeated a second time and both supernatants were pooled. The eluate was treated with 0.33 µg/µl RNaseA for 2 hours at 37°C. Samples were then decrosslinked by adding 10 µl of 4M NaCL and 1 µl of 10mg/ml proteinase K and incubated overnight at 65°C. DNA was then purified using MinElute Reaction Clean-Up kit (Qiagen, 28204).

1-5 ng of DNA was used to prepare libraries with the KAPA Hyper Prep Kit (KAPABiosystems, KK8504) and NEXTflex ChIP-Seq Barcodes for Illumina (Bioo Scientific, 514122) followed by paired-end 43bp sequencing on an Illumina NextSeq500 platform. All ChIP-seq were performed in two biological replicates, except for Rnf2 in wildtype embryos which was performed once and H3K27ac which was performed in triplicate in both wildtype and mutant embryos.

RNA-sequencing

Ten to twenty manually dechorionated 24 hpf embryos of a germline mutant incross and a germline wildtype incross were homogenized in TRIzol (Ambion, 15596018). Subsequently, the Quick RNA microprep kit (Zymo Research, R1051) was used to isolate RNA and treat the samples with DNAseI. Most samples were depleted from rRNA using the Ribo-Zero rRNA Removal Kit (Illumina, MRZH11124), followed by fragmentation, cDNA synthesis, and libraries were generated using the KAPA Hyper Prep Kit (KAPABiosystems, KK8504). Sequencing libraries were paired-end sequenced (43 bp read-length) on an Illumina NextSeq500 platform. However, two samples per genotype were generated with the TruSeq Stranded Total RNA Library Prep Kit with Ribo-Zero (Illumina, RS-122-

2201) and single-end sequenced (50 bp read-length) on an Illumina HiSeq 2500. For wildtype and *MZezh2* mutant embryos, 6 and 7 biological replicates were used, respectively.

Mass spectrometry

At 24 hpf, 50 embryos were collected, dechorionated, and resuspended by gently pipetting in 500 µl deyolking buffer (1/2 Ginzburg Fish Ringer without Calcium: 55 mM NaCl, 1.8 mM KCl, 1.25 mM NaHCO3, 1x cOmplete EDTA-free protease inhibitor cocktail from Sigma) and incubated for 5 minutes in a Thermomixer at RT at 1,100 rpm to disrupt the yolk. The samples were then centrifuged for 30 seconds at 400 g and the pellet was washed two times in 0.5 ml wash buffer (110 mM NaCl, 3.5 mM KCl, 2.7 mM CaCl2, 10mM Tris/Cl pH8.5, 1x cOmplete EDTA-free protease inhibitor cocktail from Sigma) for 2 minutes in a Thermomixer at RT and 1,100 rpm, followed by 30 seconds centrifugation at 400 g. Washed pellets were lysed in 100 µl RIPA buffer (50 mM Tris pH8.0, 150 mM NaCl, 0.1% SDS, 1% NP-40, 0.5% DOC, 20% glycerol, 1 mM Sodium Orthovanadate, 1x cOmplete EDTA-free protease inhibitor cocktails from Sigma) and sonicated for 2 cycles of 15s ON and 15s OFF on full power at 4°C on a Bioruptor (Diagenode). Samples were incubated for 1 hour on a rotating wheel at 4°C and centrifuged 10 minutes at 12,000 g and 4°C. Supernatant was flash frozen and stored at -80°C. After Bradford analysis, 100 µg protein lysate was used for FASP-SAX as previously described(68). The peptide fractions were separated on an Easy nLC 1000 (Thermo Scientific) connected to a Thermo scientific Orbitrap Fusion Tribrid mass spectrometer. MS and MS/MS spectra were recorded in a top speed modus with a run cycle of 3s using Higher- energy Collision Dissociation (HCD) fragmentation. The raw mass spectrometry data were analyzed using the MAXQuant software version 1.6.0.1 (http://www.ncbi.nlm.nih.gov/pubmed/19029910) with default settings. Data was searched against the *Danio rerio* data base (UniProt June 2017). The experiment was performed with biological triplicates for each condition.

Bioinformatics analyses

642 For ChIP-sequencing analysis, fastq files were aligned to GRCz10 zebrafish genome version using
643 BWA-MEM (version 0.7.10-r789) for paired-end reads(69). Duplicated and multimapping reads were
644 removed using samtools(70) version 1.2 and Picard tools (http://broadinstitute.github.io/picard)
645 version 2.14.1. MACS2(71) version 2.1.1 was used to call peaks from each aligned bam files using an
646 Input track from 24 hpf wild-type embryos as control sequence. Peaks separated by less than 1kb
647 distance were merged, peaks that were called using Input alone were removed from all data sets
648 using bedtools suit version 2.20.1, and the intersection between the two replicates for each
649 antibody in each condition was used to define the definitive peak sets. For visualization, fastq files
650 from duplicate ChIP-sequencing were merged, aligned as described above, and transformed into
651 bigwig alignment files using bam2bw version 1.25. Peak lists were analyzed using bedtools and
652 heatmaps were produced using deepTools plotHeatmap(72) version 2.5.3.
653 For RNA-sequencing analysis, read counts per gene were retrieve using GeneCounts quantification
654 method from STAR(73) version 2.4.0 and the GRCz10 zebrafish genome version with Ensembl
655 annotation version 87 as reference. Differential expression analysis was calculated with DESeq2(74)
656 version 1.14.1.
657 For proteomics analysis, differential expression of protein between conditions was assessed with
658 DEP(75) version 1.2.0.
659 Gene Ontology analyses on selected genes were performed using DAVID bioinformatics
660 resources(76) version 6.8 and anatomical term enrichment was done using ZEOGS(77). GSEA were
661 performed with the GSEA software from the Broad Institute(35, 36) version 3.0. To analyze the
662 proteomics data, a pre-ranked list was generated by *z*-scoring the proteins based on their $\log_2$FC
663 calculated with DEP. Only proteins with an Ensembl accession number were consider for further
664 analyses.
665
666 **Whole mount *in situ* hybridization**

667 Embryos at 24 hpf were dechorionated and fixed overnight at 4°C in 4% PFA in PBST (0.1% Tween),
668 after which they were gradually transferred to 100% methanol. Prior to ISH, embryos were gradually
669 transferred back to PBST and, subsequently, ISH was performed as described previously(78). The
670 embryos were imaged by light microscopy on a Leica MZFLIII, equipped with a DFC450 camera.
671
672 **RT-qPCR analyses**
673 Total RNA was isolated using Trizol from 20 flash-frozen dechorionated 24 hpf wildtype and *MZezh2*
674 mutant embryos cut in two with tweezers. Reverse transcription was achieved using Superscript III
675 (Invitrogen, 18080093) and poly-dT primers. Standard qPCR using SYBR Green (iQ SYBR Green
676 Supermix, BioRad, 1708880) was performed using the primers shown in Supplementary Table S2.
677 Relative expression was calculated based on expression of housekeeping genes *β-actin*. Calculations
678 were based on at least 3 independent replicates for both conditions.
679
680 **Data availability**
681 The sequencing data have been submitted to the NCBI Gene Expression Omnibus (GEO;
682 http://www.ncbi.nlm.nih.gov/geo/) under accession number GSE119070. The mass spectrometry
683 proteomics data have been deposited to the ProteomeXchange Consortium via the PRIDE(79)
684 partner repository with the dataset identifier PXD010922. Reviewers can obtain access to the
685 datasets via login information provided to the editor.
686
687
688 **Acknowledgements**
689 We thank J. Bakkers, from the Hubrecht Institute, for providing the *tbx2a*, *tbx2b*, *tbx3a*, *tbx5a*, and
690 *isl1* plasmids and J. den Hertog from the Hubrecht Institute for providing the *gsc* plasmid for ISH
691 probe generation. We thank T. Spanings and A. van der Horst from the Radboud University for
692 excellent zebrafish husbandry and E. Janssen-Megens from the Radboud University for excellent

technical support. We thank R. Lindeboom, from the Radboud University, for computational advice. We thank Dr. G.J.C. Veenstra, from the Radboud University, and his team for fruitful discussions. We thank Dr. R. Knight, from the King's College London, for his help with ISH analysis. The work was funded by the Innovative Research scheme of the Netherlands Organisation for Scientific research (www.nwo.nl, NWO-Vidi 864.12.009, NWO-Meervoud 836.13.003 L.M.K.), the Radboud University Nijmegen Medical Centre tenure track fellowship (www.radboudumc.nl, L.M.K.), the European Union's Horizon 2020 research and innovation programme under the Marie Skłodowska-Curie Grant (Agreement No. 705939, K.A.), the Howard Hughes Medical Institute and the Huntsman Cancer Institute core facilities (CA24014, B.R.C.), and the Eunice Kennedy Shriver National Institute of Child Health and Human Development of the NIH (T32HD007491, P.J.M.).

Authors' contributions

JR contributed to conception and design of the study, performed and analyzed experiments, and wrote and edited the manuscript. NDC contributed to conception and design of the study, performed RNA extraction and ISH imaging, and edited the manuscript. MA performed library preparation and RT-qPCR. KA performed Western blot experiments, acquired funding, and edited the manuscript. DME assisted with bioinformatics analyses and edited the manuscript. PJM and BRC performed RNA-seq experiments and analysis, acquired funding, and edited the manuscript. PWTCJ and MV performed proteomics experiments and analysis and edited the manuscript. LMK contributed to conception and design of the study, performed experiments, acquired funding, and wrote and edited the manuscript.

Competing interests

719 The authors declare no competing interests.

720

721

722 **References**

723 1. Brock HW, Fisher CL. Maintenance of gene expression patterns. Developmental
724 dynamics : an official publication of the American Association of Anatomists. 2005;232(3):633-55.
725 2. Zhu P, Li G. Structural insights of nucleosome and the 30-nm chromatin fiber.
726 Current opinion in structural biology. 2016;36:106-15.
727 3. Li G, Reinberg D. Chromatin higher-order structures and gene regulation. Current
728 opinion in genetics & development. 2011;21(2):175-86.
729 4. Kennison JA. The Polycomb and trithorax group proteins of Drosophila: trans-
730 regulators of homeotic gene function. Annual review of genetics. 1995;29:289-303.
731 5. Schuettengruber B, Bourbon HM, Di Croce L, Cavalli G. Genome Regulation by
732 Polycomb and Trithorax: 70 Years and Counting. Cell. 2017;171(1):34-57.
733 6. Chittock EC, Latwiel S, Miller TC, Muller CW. Molecular architecture of polycomb
734 repressive complexes. Biochemical Society transactions. 2017;45(1):193-205.
735 7. Mikkelsen TS, Ku M, Jaffe DB, Issac B, Lieberman E, Giannoukos G, Alvarez P,
736 Brockman W, Kim TK, Koche RP, Lee W, Mendenhall E, O'Donovan A, Presser A, Russ C, Xie X,
737 Meissner A, Wernig M, Jaenisch R, Nusbaum C, et al. Genome-wide maps of chromatin state in
738 pluripotent and lineage-committed cells. Nature. 2007;448(7153):553-60.
739 8. Margueron R, Li G, Sarma K, Blais A, Zavadil J, Woodcock CL, Dynlacht BD, Reinberg
740 D. Ezh1 and Ezh2 maintain repressive chromatin through different mechanisms. Molecular cell.
741 2008;32(4):503-18.
742 9. Shen X, Liu Y, Hsu YJ, Fujiwara Y, Kim J, Mao X, Yuan GC, Orkin SH. EZH1 mediates
743 methylation on histone H3 lysine 27 and complements EZH2 in maintaining stem cell identity and
744 executing pluripotency. Molecular cell. 2008;32(4):491-502.
745 10. Gao Z, Zhang J, Bonasio R, Strino F, Sawai A, Parisi F, Kluger Y, Reinberg D. PCGF
746 homologs, CBX proteins, and RYBP define functionally distinct PRC1 family complexes. Molecular
747 cell. 2012;45(3):344-56.
748 11. Kloet SL, Makowski MM, Baymaz HI, van Voorthuijsen L, Karemaker ID, Santanach A,
749 Jansen P, Di Croce L, Vermeulen M. The dynamic interactome and genomic targets of Polycomb
750 complexes during stem-cell differentiation. Nature structural & molecular biology. 2016;23(7):682-
751 90.

12. He J, Shen L, Wan M, Taranova O, Wu H, Zhang Y. Kdm2b maintains murine embryonic stem cell status by recruiting PRC1 complex to CpG islands of developmental genes. Nature cell biology. 2013;15(4):373-84.

13. Loubiere V, Delest A, Thomas A, Bonev B, Schuettengruber B, Sati S, Martinez AM, Cavalli G. Coordinate redeployment of PRC1 proteins suppresses tumor formation during Drosophila development. Nature genetics. 2016;48(11):1436-42.

14. Tavares L, Dimitrova E, Oxley D, Webster J, Poot R, Demmers J, Bezstarosti K, Taylor S, Ura H, Koide H, Wutz A, Vidal M, Elderkin S, Brockdorff N. RYBP-PRC1 complexes mediate H2A ubiquitylation at polycomb target sites independently of PRC2 and H3K27me3. Cell. 2012;148(4):664-78.

15. Klymenko T, Muller J. The histone methyltransferases Trithorax and Ash1 prevent transcriptional silencing by Polycomb group proteins. EMBO reports. 2004;5(4):373-7.

16. Schmitges FW, Prusty AB, Faty M, Stutzer A, Lingaraju GM, Aiwazian J, Sack R, Hess D, Li L, Zhou S, Bunker RD, Wirth U, Bouwmeester T, Bauer A, Ly-Hartig N, Zhao K, Chan H, Gu J, Gut H, Fischle W, et al. Histone methylation by PRC2 is inhibited by active chromatin marks. Molecular cell. 2011;42(3):330-41.

17. Santos-Rosa H, Schneider R, Bannister AJ, Sherriff J, Bernstein BE, Emre NC, Schreiber SL, Mellor J, Kouzarides T. Active genes are tri-methylated at K4 of histone H3. Nature. 2002;419(6905):407-11.

18. Creyghton MP, Cheng AW, Welstead GG, Kooistra T, Carey BW, Steine EJ, Hanna J, Lodato MA, Frampton GM, Sharp PA, Boyer LA, Young RA, Jaenisch R. Histone H3K27ac separates active from poised enhancers and predicts developmental state. Proceedings of the National Academy of Sciences of the United States of America. 2010;107(50):21931-6.

19. O'Carroll D, Erhardt S, Pagani M, Barton SC, Surani MA, Jenuwein T. The polycomb-group gene Ezh2 is required for early mouse development. Molecular and cellular biology. 2001;21(13):4330-6.

20. Faust C, Lawson KA, Schork NJ, Thiel B, Magnuson T. The Polycomb-group gene eed is required for normal morphogenetic movements during gastrulation in the mouse embryo. Development. 1998;125(22):4495-506.

21. Pasini D, Bracken AP, Jensen MR, Lazzerini Denchi E, Helin K. Suz12 is essential for mouse development and for EZH2 histone methyltransferase activity. The EMBO journal. 2004;23(20):4061-71.

22. Voncken JW, Roelen BA, Roefs M, de Vries S, Verhoeven E, Marino S, Deschamps J, van Lohuizen M. Rnf2 (Ring1b) deficiency causes gastrulation arrest and cell cycle inhibition.

786 Proceedings of the National Academy of Sciences of the United States of America. 2003;100(5):2468-
787 73.
788 23. Lindeman LC, Andersen IS, Reiner AH, Li N, Aanes H, Ostrup O, Winata C, Mathavan
789 S, Muller F, Alestrom P, Collas P. Prepatterning of developmental gene expression by modified
790 histones before zygotic genome activation. Developmental cell. 2011;21(6):993-1004.
791 24. Murphy PJ, Wu SF, James CR, Wike CL, Cairns BR. Placeholder Nucleosomes Underlie
792 Germline-to-Embryo DNA Methylation Reprogramming. Cell. 2018;172(5):993-1006 e13.
793 25. Potok ME, Nix DA, Parnell TJ, Cairns BR. Reprogramming the maternal zebrafish
794 genome after fertilization to match the paternal methylation pattern. Cell. 2013;153(4):759-72.
795 26. Vastenhouw NL, Zhang Y, Woods IG, Imam F, Regev A, Liu XS, Rinn J, Schier AF.
796 Chromatin signature of embryonic pluripotency is established during genome activation. Nature.
797 2010;464(7290):922-6.
798 27. Dupret B, Volkel P, Vennin C, Toillon RA, Le Bourhis X, Angrand PO. The histone
799 lysine methyltransferase Ezh2 is required for maintenance of the intestine integrity and for caudal
800 fin regeneration in zebrafish. Biochimica et biophysica acta. 2017;1860(10):1079-93.
801 28. San B, Chrispijn ND, Wittkopp N, van Heeringen SJ, Lagendijk AK, Aben M, Bakkers J,
802 Ketting RF, Kamminga LM. Normal formation of a vertebrate body plan and loss of tissue
803 maintenance in the absence of ezh2. Scientific reports. 2016;6:24658.
804 29. Zhong Y, Ye Q, Chen C, Wang M, Wang H. Ezh2 promotes clock function and
805 hematopoiesis independent of histone methyltransferase activity in zebrafish. Nucleic acids
806 research. 2018;46(7):3382-99.
807 30. Ciruna B, Weidinger G, Knaut H, Thisse B, Thisse C, Raz E, Schier AF. Production of
808 maternal-zygotic mutant zebrafish by germ-line replacement. Proceedings of the National Academy
809 of Sciences of the United States of America. 2002;99(23):14919-24.
810 31. Le Faou P, Volkel P, Angrand PO. The zebrafish genes encoding the Polycomb
811 repressive complex (PRC) 1. Gene. 2011;475(1):10-21.
812 32. Piunti A, Shilatifard A. Epigenetic balance of gene expression by Polycomb and
813 COMPASS families. Science. 2016;352(6290):aad9780.
814 33. Rickels R, Shilatifard A. Enhancer Logic and Mechanics in Development and Disease.
815 Trends in cell biology. 2018;28(8):608-30.
816 34. King AD, Huang K, Rubbi L, Liu S, Wang CY, Wang Y, Pellegrini M, Fan G. Reversible
817 Regulation of Promoter and Enhancer Histone Landscape by DNA Methylation in Mouse Embryonic
818 Stem Cells. Cell reports. 2016;17(1):289-302.

819 35. Mootha VK, Lindgren CM, Eriksson KF, Subramanian A, Sihag S, Lehar J, Puigserver P,
820 Carlsson E, Ridderstrale M, Laurila E, Houstis N, Daly MJ, Patterson N, Mesirov JP, Golub TR, Tamayo
821 P, Spiegelman B, Lander ES, Hirschhorn JN, Altshuler D, et al. PGC-1alpha-responsive genes involved
822 in oxidative phosphorylation are coordinately downregulated in human diabetes. Nature genetics.
823 2003;34(3):267-73.
824 36. Subramanian A, Tamayo P, Mootha VK, Mukherjee S, Ebert BL, Gillette MA,
825 Paulovich A, Pomeroy SL, Golub TR, Lander ES, Mesirov JP. Gene set enrichment analysis: a
826 knowledge-based approach for interpreting genome-wide expression profiles. Proceedings of the
827 National Academy of Sciences of the United States of America. 2005;102(43):15545-50.
828 37. Mallo M, Alonso CR. The regulation of Hox gene expression during animal
829 development. Development. 2013;140(19):3951-63.
830 38. Prince VE, Joly L, Ekker M, Ho RK. Zebrafish hox genes: genomic organization and
831 modified colinear expression patterns in the trunk. Development. 1998;125(3):407-20.
832 39. Thisse BT, C. Fast Release Clones: A High Throughput Expression Analysis. ZFIN Direct
833 Data Submission (http://zfinorg). 2004.
834 40. Ribeiro I, Kawakami Y, Buscher D, Raya A, Rodriguez-Leon J, Morita M, Rodriguez
835 Esteban C, Izpisua Belmonte JC. Tbx2 and Tbx3 regulate the dynamics of cell proliferation during
836 heart remodeling. PloS one. 2007;2(4):e398.
837 41. Tamura K, Yonei-Tamura S, Izpisua Belmonte JC. Differential expression of Tbx4 and
838 Tbx5 in Zebrafish fin buds. Mechanisms of development. 1999;87(1-2):181-4.
839 42. Dyer C, Linker C, Graham A, Knight R. Specification of sensory neurons occurs
840 through diverse developmental programs functioning in the brain and spinal cord. Developmental
841 dynamics : an official publication of the American Association of Anatomists. 2014;243(11):1429-39.
842 43. Heisenberg CP, Brennan C, Wilson SW. Zebrafish aussicht mutant embryos exhibit
843 widespread overexpression of ace (fgf8) and coincident defects in CNS development. Development.
844 1999;126(10):2129-40.
845 44. Zhang R, Knapp M, Suzuki K, Kajioka D, Schmidt JM, Winkler J, Yilmaz O, Pleschka M,
846 Cao J, Kockum CC, Barker G, Holmdahl G, Beaman G, Keene D, Woolf AS, Cervellione RM, Cheng W,
847 Wilkins S, Gearhart JP, Sirchia F, et al. ISL1 is a major susceptibility gene for classic bladder exstrophy
848 and a regulator of urinary tract development. Scientific reports. 2017;7:42170.
849 45. Chrispijn ND, Andralojc KM, Castenmiller C, Kamminga LM. Gene expression profile
850 of a selection of Polycomb Group genes during zebrafish embryonic and germ line development.
851 PloS one. 2018;13(7):e0200316.

852 46. Sun XJ, Xu PF, Zhou T, Hu M, Fu CT, Zhang Y, Jin Y, Chen Y, Chen SJ, Huang QH, Liu TX,
853 Chen Z. Genome-wide survey and developmental expression mapping of zebrafish SET domain-
854 containing genes. PloS one. 2008;3(1):e1499.
855 47. White RJ, Collins JE, Sealy IM, Wali N, Dooley CM, Digby Z, Stemple DL, Murphy DN,
856 Billis K, Hourlier T, Fullgrabe A, Davis MP, Enright AJ, Busch-Nentwich EM. A high-resolution mRNA
857 expression time course of embryonic development in zebrafish. eLife. 2017;6.
858 48. Hagarman JA, Motley MP, Kristjansdottir K, Soloway PD. Coordinate regulation of
859 DNA methylation and H3K27me3 in mouse embryonic stem cells. PloS one. 2013;8(1):e53880.
860 49. Peters AH, Kubicek S, Mechtler K, O'Sullivan RJ, Derijck AA, Perez-Burgos L,
861 Kohlmaier A, Opravil S, Tachibana M, Shinkai Y, Martens JH, Jenuwein T. Partitioning and plasticity of
862 repressive histone methylation states in mammalian chromatin. Molecular cell. 2003;12(6):1577-89.
863 50. Reddington JP, Perricone SM, Nestor CE, Reichmann J, Youngson NA, Suzuki M,
864 Reinhardt D, Dunican DS, Prendergast JG, Mjoseng H, Ramsahoye BH, Whitelaw E, Greally JM, Adams
865 IR, Bickmore WA, Meehan RR. Redistribution of H3K27me3 upon DNA hypomethylation results in de-
866 repression of Polycomb target genes. Genome biology. 2013;14(3):R25.
867 51. McGinnis W, Tickle C. Pattern formation and developmental mechanisms: good
868 mileage from comparative studies in cell biology, gene regulation, development and evolution.
869 Current opinion in genetics & development. 2005;15(4):355-7.
870 52. Laursen KB, Mongan NP, Zhuang Y, Ng MM, Benoit YD, Gudas LJ. Polycomb
871 recruitment attenuates retinoic acid-induced transcription of the bivalent NR2F1 gene. Nucleic acids
872 research. 2013;41(13):6430-43.
873 53. Zhang Y, Liang J, Li Q. Coordinated regulation of retinoic acid signaling pathway by
874 KDM5B and polycomb repressive complex 2. Journal of cellular biochemistry. 2014;115(9):1528-38.
875 54. Cunningham TJ, Zhao X, Sandell LL, Evans SM, Trainor PA, Duester G. Antagonism
876 between retinoic acid and fibroblast growth factor signaling during limb development. Cell reports.
877 2013;3(5):1503-11.
878 55. Grandel H, Brand M. Zebrafish limb development is triggered by a retinoic acid signal
879 during gastrulation. Developmental dynamics : an official publication of the American Association of
880 Anatomists. 2011;240(5):1116-26.
881 56. Lupo G, Liu Y, Qiu R, Chandraratna RA, Barsacchi G, He RQ, Harris WA. Dorsoventral
882 patterning of the Xenopus eye: a collaboration of Retinoid, Hedgehog and FGF receptor signaling.
883 Development. 2005;132(7):1737-48.

884 57. Marsh-Armstrong N, McCaffery P, Gilbert W, Dowling JE, Drager UC. Retinoic acid is
885 necessary for development of the ventral retina in zebrafish. Proceedings of the National Academy
886 of Sciences of the United States of America. 1994;91(15):7286-90.
887 58. Maves L, Kimmel CB. Dynamic and sequential patterning of the zebrafish posterior
888 hindbrain by retinoic acid. Developmental biology. 2005;285(2):593-605.
889 59. White RJ, Nie Q, Lander AD, Schilling TF. Complex regulation of cyp26a1 creates a
890 robust retinoic acid gradient in the zebrafish embryo. PLoS biology. 2007;5(11):e304.
891 60. Samarut E, Fraher D, Laudet V, Gibert Y. ZebRA: An overview of retinoic acid
892 signaling during zebrafish development. Biochimica et biophysica acta. 2015;1849(2):73-83.
893 61. van der Velden YU, Wang L, van Lohuizen M, Haramis AP. The Polycomb group
894 protein Ring1b is essential for pectoral fin development. Development. 2012;139(12):2210-20.
895 62. Joubin K, Stern CD. Molecular interactions continuously define the organizer during
896 the cell movements of gastrulation. Cell. 1999;98(5):559-71.
897 63. Stachel SE, Grunwald DJ, Myers PZ. Lithium perturbation and goosecoid expression
898 identify a dorsal specification pathway in the pregastrula zebrafish. Development. 1993;117(4):1261-
899 74.
900 64. Westerfield M. The zebrafish book. A guide for the laboratory use of zebrafish
901 (Danio rerio). 4th ed., Univ. of Oregon Press, Eugene. 2000.
902 65. Kimmel CB, Ballard WW, Kimmel SR, Ullmann B, Schilling TF. Stages of embryonic
903 development of the zebrafish. Developmental dynamics : an official publication of the American
904 Association of Anatomists. 1995;203(3):253-310.
905 66. Pauls S, Geldmacher-Voss B, Campos-Ortega JA. A zebrafish histone variant H2A.F/Z
906 and a transgenic H2A.F/Z:GFP fusion protein for in vivo studies of embryonic development.
907 Development genes and evolution. 2001;211(12):603-10.
908 67. Krovel AV, Olsen LC. Expression of a vas::EGFP transgene in primordial germ cells of
909 the zebrafish. Mechanisms of development. 2002;116(1-2):141-50.
910 68. Wisniewski JR, Ostasiewicz P, Mann M. High recovery FASP applied to the proteomic
911 analysis of microdissected formalin fixed paraffin embedded cancer tissues retrieves known colon
912 cancer markers. Journal of proteome research. 2011;10(7):3040-9.
913 69. Li H, Durbin R. Fast and accurate short read alignment with Burrows-Wheeler
914 transform. Bioinformatics. 2009;25(14):1754-60.
915 70. Li H, Handsaker B, Wysoker A, Fennell T, Ruan J, Homer N, Marth G, Abecasis G,
916 Durbin R, Genome Project Data Processing S. The Sequence Alignment/Map format and SAMtools.
917 Bioinformatics. 2009;25(16):2078-9.

71. Zhang Y, Liu T, Meyer CA, Eeckhoute J, Johnson DS, Bernstein BE, Nusbaum C, Myers RM, Brown M, Li W, Liu XS. Model-based analysis of ChIP-Seq (MACS). Genome biology. 2008;9(9):R137.

72. Ramirez F, Ryan DP, Gruning B, Bhardwaj V, Kilpert F, Richter AS, Heyne S, Dundar F, Manke T. deepTools2: a next generation web server for deep-sequencing data analysis. Nucleic acids research. 2016;44(W1):W160-5.

73. Dobin A, Davis CA, Schlesinger F, Drenkow J, Zaleski C, Jha S, Batut P, Chaisson M, Gingeras TR. STAR: ultrafast universal RNA-seq aligner. Bioinformatics. 2013;29(1):15-21.

74. Love MI, Huber W, Anders S. Moderated estimation of fold change and dispersion for RNA-seq data with DESeq2. Genome biology. 2014;15(12):550.

75. Zhang X, Smits AH, van Tilburg GB, Ovaa H, Huber W, Vermeulen M. Proteome-wide identification of ubiquitin interactions using UbIA-MS. Nature protocols. 2018;13(3):530-50.

76. Huang da W, Sherman BT, Lempicki RA. Systematic and integrative analysis of large gene lists using DAVID bioinformatics resources. Nature protocols. 2009;4(1):44-57.

77. Prykhozhij SV, Marsico A, Meijsing SH. Zebrafish Expression Ontology of Gene Sets (ZEOGS): a tool to analyze enrichment of zebrafish anatomical terms in large gene sets. Zebrafish. 2013;10(3):303-15.

78. Houwing S, Kamminga LM, Berezikov E, Cronembold D, Girard A, van den Elst H, Filippov DV, Blaser H, Raz E, Moens CB, Plasterk RH, Hannon GJ, Draper BW, Ketting RF. A role for Piwi and piRNAs in germ cell maintenance and transposon silencing in Zebrafish. Cell. 2007;129(1):69-82.

79. Vizcaino JA, Csordas A, del-Toro N, Dianes JA, Griss J, Lavidas I, Mayer G, Perez-Riverol Y, Reisinger F, Ternent T, Xu QW, Wang R, Hermjakob H. 2016 update of the PRIDE database and its related tools. Nucleic acids research. 2016;44(D1):D447-56.

943 **Supplementary Figure Legends**

944

945 **Supplementary Fig. 1. Analysis of Ezh2, H3K27me3, and Rnf2 binding in wildtype and *MZezh2***
946 **mutant (*MZezh2*$^{-/-}$) embryos at 24 hpf.** (**A**) Venn diagrams presenting the overlap between Ezh2
947 (blue) and H3K27me3 (red) and between Ezh2 (blue) and Rnf2 (purple) peaks detected in 24 hpf
948 wildtype embryos. (**B**) UCSC browser snapshots of three genomic loci depicting Ezh2, H3K27me3,
949 and Rnf2 binding after ChIP-seq in *MZezh2*$^{-/-}$ embryos compared to wildtype embryos at 24 hpf.
950 Colors represent ChIP-seq for different proteins with blue: Ezh2, red: H3K27me3, purple: Rnf2, and
951 grey: Input control. (**C**) UCSC browser snapshots of two genomic loci (chr13:1,134,029-1,134,242 and
952 chr13:40,038,792-40,038,959) representative of a-specific binding present on repeat regions for all
953 tested epigenetic marks after ChIP-seq in *MZezh2*$^{-/-}$ and wildtype embryos at 24 hpf. Colors are as in
954 (**A**). (**D**) Heatmaps for Ezh2, H3K27me3, Rnf2, H3K4me3, and H3K27ac RPKM-normalized coverage
955 after ChIP-seq in 24 hpf wildtype embryos. Windows of 20 kb regions at all H3K27me3 and Ezh2
956 peaks in 24 hpf wildtype embryos are shown. An input track obtained from 24 hpf wildtype embryos
957 was used as control. Colors are as in (**A**). (**E**) Example of *ezh2*$^{(hu5670)}$ genotyping results after nested
958 PCR, RsaI restriction, and gel electrophoresis in *MZezh2* wildtype (*MZezh2*$^{+/+}$), *MZezh2* heterozygous
959 (*MZezh2*$^{+/-}$), and *MZezh2* mutant (*MZezh2*$^{-/-}$) embryos.

960

961 **Supplementary Fig. 2. Decrease of H3K27ac binding in *MZezh2* mutant (*MZezh2*$^{-/-}$) embryos at 24**
962 **hpf.** (**A**) Number of peaks called after H3K27ac ChIP-seq in wildtype and *MZezh2*$^{-/-}$ embryos at 24
963 hpf. Dark and light blue boxes show peaks detected in both wildtype and *MZezh2*$^{-/-}$ embryos or
964 specific to one condition, respectively. Each peak set was obtained by the intersection of at least two
965 out of three independent replicates. Dark and light blue represent peaks shared by the two
966 conditions and specific from one condition, respectively. (**B**) Box plots of H3K27ac3 RPKM-
967 normalized coverage after ChIP-seq in wildtype and in *MZezh2*$^{-/-}$ embryos at 24 hpf. The input
968 control was obtained from wildtype embryos at 24 hpf. Coverages were calculated based on

969 enriched peaks detected in both wildtype and *MZezh2*$^{-/-}$ embryos (shared), specific for *MZezh2*$^{-/-}$

970 embryos, and specific for wildtype embryos. Colors are as in (**a**). t-test: *** *P*-value < 0.001.

971

972 **Supplementary Fig. 3. RNA-seq and proteomics analysis in *MZezh2* mutant (*MZezh2*$^{-/-}$) embryos at**

973 **24 hpf.** (**A**) Analysis of anatomical terms associated with genes upregulated and downregulated in

974 *MZezh2*$^{-/-}$ embryos compared to wildtype embryos at 24 hpf. (**B**) Schematic representation of

975 changes in protein expression level of PRC2 (left) and canonical PRC1 (right) subunits in *MZezh2*$^{-/-}$

976 compared to wildtype embryos at 24 hpf. Dark red: $\log_2$fold-change ≥ 1 and *P*-value ≤ 0.05, light red:

977 $\log_2$fold-change ≥ 0, turquoise: $\log_2$fold-change ≤ 0, grey: protein not detected.